A Method to Calculate Uncertainty of Empirical Compressor Maps with the Consideration of Extrapolation Effect and Choice of Training Data

Although compressor maps are powerful tools to estimate compressor power consumption quickly, their ability to extrapolate outside their training data range is always questioned. In order to quantify the effect of extrapolation, a method to calculate the uncertainty of compressor map outputs is developed in this paper. The method considers 4 major components of uncertainties due to various sources such as measurement uncertainties of training data and equation of state. The change of the predicted map uncertainty with the degree of extrapolation and the map accuracy are shown for 8 different compressor maps. The results indicate that the uncertainty from model random error increases significantly as the maps extrapolate though extrapolation does not necessarily imply inaccurate compressor map outputs. The results also show that the uncertainty due to training data is the most significant component of uncertainties when the maps are not extrapolated.

Introduction and Literature Review

Compressor models are widely used in specifying the performance of compressors by manufacturers for design purposes of compressors as well as for vapor compression system simulation. When models are built for compressor designs, deterministic models such as e.g. Wang et al. (2008), Bell et al. (2012), Gall et al. (2015) and Ibsaine et al. (2016) are used because the models give them flexibility to optimize a compressor design by tuning the geometry of the compressors and compressor valves and allows the investigators to study the compressor dynamics in details. However, modelers of thermal systems using compressors do not need the flexibility because changes of compressor geometry are usually not concerns of the system modelers (Ding 2007), nor do they need the study of the compressor dynamics because heat exchanger dynamics are usually more important in their applications (Rasmussen 2012). While models of some types of compressors can be simplified for their uses as subsystem models (Wang et al. 2000), others who cannot simplify the deterministic models such as ones of scroll compressors prefer to use simplified compressor models trained by experimental data. This speeds up their models which require multiple runs

of the compressor model for one run of their system models (Park et al. 2001; Zakula et al. 2011; Cheung and Braun 2013; Heo et al. 2013). The simplest compressor map has standard forms (e.g. AHRI Standard 540 (AHRI 2004), EN Standard 12900 (CEN 2013)) that can be constructed easily by linear regression with measurements of compressor suction and discharge pressure in calorimeter tests and are commonly used by compressor manufacturers to describe their compressor performance in specifications and reports (AHRI, 2016).

The performance of mappings is commonly expressed in terms of the accuracy of the maps at training data points. This can be easily done and therefore used widely for conventional compressors (e.g. Jähnig et al. 2000; Winandy et al. 2002), variable speed compressors (e.g. Shao et al. 2004), as well as for compressors with injection (e.g. Navarro et al. 2013; Bach et al. 2015; Dardenne et al. 2015).

Although the performance accessed by prediction accuracy at training data points is easy for readers to understand, they do not account for the effect of the measurement uncertainty of the training data. They also do not specify the effect of the choice of training data to the accuracy of the maps (e.g. the change of map accuracy due to the change of the training data set). It is typically unclear if the maps are accurate outside their training data range before any experimental validation, and this lack of knowledge may cost opportunities in compressor model development such as the possibility to reduce the number of calorimeter tests with correct choices of calorimeter test conditions and the option of validation of compressor map outputs for out-of-range operation without extra testing. This also hinders the research development using compressor maps such as cold climate heat pump (Caskey et al. 2012) and faulted vapor compression systems (Shen et al. 2009) which involves the use of compressor maps at out-of-range operation.

Few research papers investigate the issue of map performance outside the range of training data. Jähnig et al (2000) conducted a rigorous study in which they showed that map performance outside of the training data range can drastically differ from the performance within the training data range. The authors did extra tests to define the extrapolation accuracy of the map to be within 10% of the measurement when the evaporating and condensing temperature lied within 10 K (18°R) from the extremes in the training data, but it is unknown how the magnitude of the temperature difference 10 K (18°R) is coupled with the range of the saturation temperature in the training data. Li (2012) did a similar study for its scroll and reciprocating compressor model. Aute et al. (2015) compared various compressor modeling methods and used Monte

Carlo method to calculate the uncertainty of 10-coefficient compressor maps, but its method from Coleman and Steele (2009) does not involve the difference between model training data and model inputs and cannot account for the effect of extrapolation to model uncertainties well. Their method also requires more than 1,000 runs of the map and its training process to calculate the uncertainty per data point is not very feasible for most applications.

It is usually believed that extrapolation error might be reduced by using deterministic models, such as ones in Wang et al. (2008), Bell et al. (2012), and Molinaroli et al. (2017), which are tuned or scaled towards the experimental data. However, these deterministic models are often not used in developments that require quantification of extrapolation errors because of the aforementioned reasons, and another approach is needed to quantify the potential extrapolation error.

To simplify the quantification of extrapolation error for empirical compressor maps, Cheung and Bach (2015) proposed a method to break up overall compressor power consumption uncertainty into four contribution components. The authors compared the actual accuracy of the map to the sum of the uncertainty contribution components and found that both increase if the number of training data points is decreased. Uncertainty was found to increase with increasing distance from the nearest training data point. Bach and Cheung (2015) extended the method in Cheung and Bach (2015) towards data from a vapor injected compressor. However, both papers were developed on either simulation results only or the performance of specialized models. A more rigorous method that is validated by experimental results and a more general method of compressor map uncertainty prediction is therefore needed.

This paper focuses on the development and application of a rigorous approach taking into account all major aspects and sources of the uncertainties involved in 10-coefficient compressor map in AHRI Standard 540 (AHRI 2010) that predicts compressor power consumption. The map is widely used in the community for various applications (e.g. use of the compressor maps in reports to compare performance of compressors using various refrigerants from different manufacturers in AHRI 2016; use of the compressor map in cold climate heat pump studies in Caskey et al. 2012; use of the compressor map for vapor compression system design in Rice and Jackson 2005; use of the compressor map for faulted vapor compression systems in Shen et al. 2009; study of the uncertainty of the compressor map with a numerical approach in Aute et al. 2015) and are useful to illustrate the quantification of extrapolation effect by

uncertainty calculation. In particular, it breaks out the effect of different uncertainty components, including pressure measurement, equation of state, model random error, training data, and outputs. This breakdown allows to specify the major sources of uncertainty and their effects due to changes in the training data, which can be used to simplify the calculation of these components further in future works.

Linear Regression for 10-Coefficient Compressor Maps

To understand how uncertainty of compressor map can be affected by its training data, it is necessary to understand the training of the coefficients in 10-coefficient compressor maps by linear regression. Linear regression estimates parameters in a linear model of a system with some nonlinear behavior, and its true model can be mathematically written as Eq. (1) (Montgomery 2005).

$$y_{true} = \vec{x}^T \vec{\beta}_{true} + \varepsilon \tag{1}$$

Eq. (1) shows a linear model which the true value of a dependent variable y equals to the dot product of an independent variable vector $\vec{x}$ and a vector of true coefficients $\vec{\beta}_{true}$ with an error ε between the model and the system. However, it is impossible to obtain the true values of the parameter vector because it is impossible to obtain every possible pairs of dependent variables and independent variable vectors in the system. Each pair of dependent variable and independent variable vector is a data point, and the model coefficients can only be estimated from a finite set of observations of data points from the system. The resultant model only contains estimates of the coefficients and can only give estimates of the dependent variable rather than its true values as shown in Eq. (2).

$$\hat{y} = \vec{x}^T \hat{\vec{\beta}} \tag{2}$$

The estimated coefficients in Eq. (2) can be calculated from measurement of independent and dependent variables in a system as shown in Eq. (3).

$$\hat{\vec{\beta}} = (X_{train}^T X_{train})^{-1} X_{train}^T \vec{y}_{train} \tag{3}$$

Variables with the subscript train in Eq. (3) represent training data of the model. The matrix X_{train} in Eq. (3) is formed by the independent variable vectors in all data points inside the training data as shown in Eq. (4).

$$X_{train} = [\vec{x}_{train,1} \quad \cdots \quad \vec{x}_{train,i} \quad \cdots \quad \vec{x}_{train,n}]^T \tag{4}$$

The vector of dependent variables of training data in Eq. (3) is also defined in a similar manner as Eq. (5) .

$$\vec{y}_{train} = [y_{train,1} \quad \cdots \quad y_{train,i} \quad \cdots \quad y_{train,n}]^T \tag{5}$$

A 10-coefficient compressor map that estimates compressor power consumption is a cubic polynomial that depends on dew point temperature values at compressor suction and discharge as shown in Eq. (6).

$$\widehat{W}_{comp} = \beta_0 + \beta_1 T_{dew,suc} + \beta_2 T_{dew,dis} + \beta_3 T^2_{dew,suc} + \beta_4 T_{dew,suc} T_{dew,dis} \tag{6}$$

$$+ \beta_5 T^2_{dew,dis} + \beta_6 T^3_{dew,suc} + \beta_7 T^2_{dew,suc} T_{dew,dis}$$

$$+ \beta_8 T_{dew,suc} T^2_{dew,dis} + \beta_9 T^3_{dew,dis}$$

Although the polynomial is not a simple linear equation, its empirical coefficients can still be estimated by linear regression. To estimate the parameters in the 10-coefficient compressor map by linear regression, the map is converted to the equation form Eq. (2) by using the independent variable vector in Eq. (7) and the power consumption as the dependent variable.

$$\vec{x} \tag{7}$$
$$= [1 \quad T_{dew,suc} \quad T_{dew,dis} \quad T^2_{dew,suc} \quad T_{dew,suc} T_{dew,dis} \quad T^2_{dew,dis} \quad T^3_{dew,suc} \quad T^2_{dew,suc} T_{dew,dis} \quad T_{dew,suc} T^2_{dew,dis} \quad T^3_{dew,dis}]^T$$

The coefficients in Eq. (6) can then be calculated by Eq. (3). Occasionally the inversion of matrices in Eq. (3) may yield incorrect answers in computers due to numerical round-off errors, and normalization of Eq. (7) may be needed to calculate the correct parameters. In this case, the normalized vector $\vec{x}$ should be used in all uncertainty calculation methods in this paper in order to calculate the correct uncertainties and estimation.

Although the map uses dew point temperature at compressor suction and discharge, they are not measured directly from the compressor. In reality, only refrigerant pressure values at compressor suction and discharge are measured, and then converted to compressor suction and discharge dew point temperature before being used by the maps to calculate compressor power consumption.

Method to Calculate Uncertainty of Compressor Map Output

Uncertainty of the compressor map output quantifies the potential difference between the true values of the output to the map outputs. The sources of uncertainty propagated to the map output are illustrated in Figure 1.
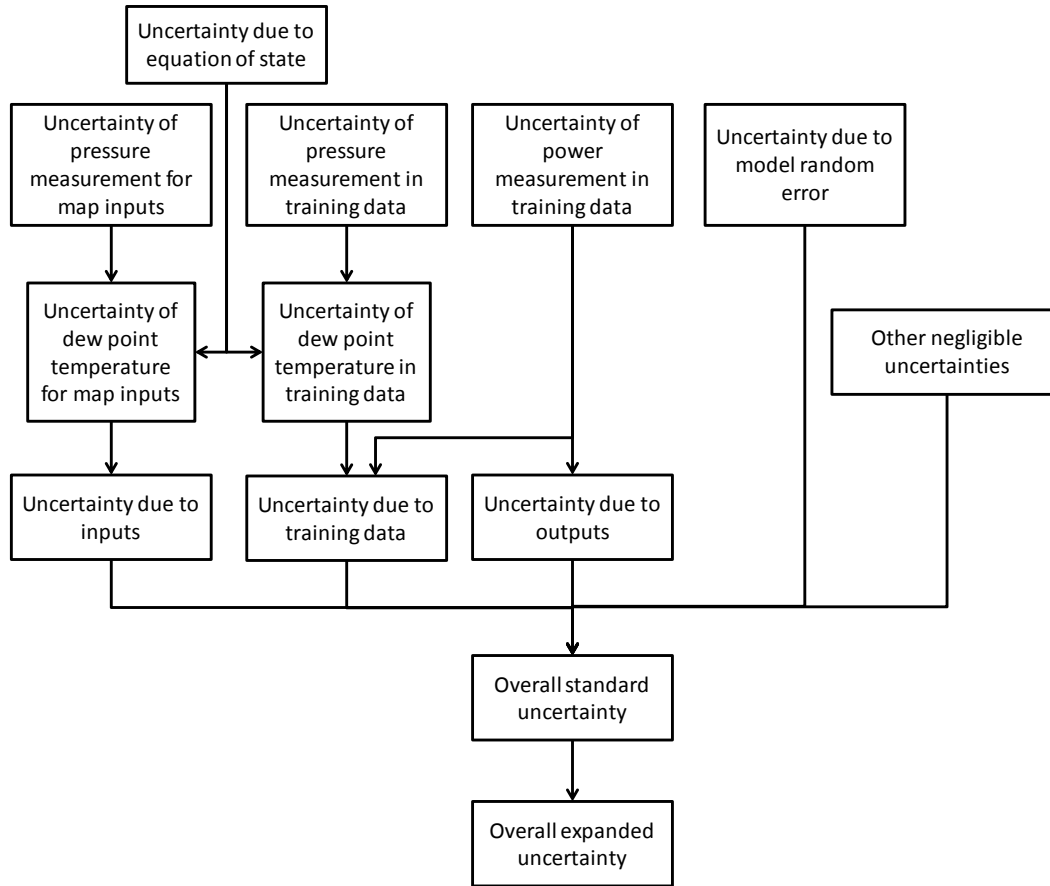
Figure 1: Flowchart of uncertainty propagation to the compressor map output

Although most people only consider the propagation of uncertainty of measurement at map inputs as the uncertainty of the map output, the propagation of uncertainty starts with measurement values in both the map inputs and the training data. The power and pressure values in the map inputs and the training data carry measurement uncertainties and propagate to the map outputs as they are used in the estimation and the training process. Because the pressure values are converted to dew point temperature before use and the dew point temperatures are calculated from pressure measurements by the equation of state of the refrigerant, the uncertainty of the equation of state propagates to the map output through the estimation and the training process. The propagation of uncertainties from the input variables when a user uses the map is the uncertainty due to inputs, and the propagation of uncertainties from training data during the map training process forms the uncertainty due to training data. During the creation of the map, it is impossible for a user to confirm if a map is identical to the corresponding true mathematical relationship and to use all possible data points within the applicable range of the map. There are always some uncertainties in the mathematical structure of the map and its estimated coefficients even if there are no uncertainties in the

measurement and equation of state, and it is proposed to account for this type of uncertainty by calculating the uncertainty due to model random error. Since the map is trained by measured values of the variables, the uncertainty components only account for the uncertainty between the map estimation and the corresponding measurement. However, the uncertainty of a sensor is the uncertainty between the measurement and the corresponding true value, and hence the uncertainty of a map output should be defined similarly as the uncertainty between the estimation and the corresponding true value, and an uncertainty component called the uncertainty due to outputs is introduced to satisfy this definition. . These uncertainties together form the uncertainty due to inputs, the uncertainty due to training data, the uncertainty due to model random error, and the uncertainty due to outputs. The imperfection of the cubic compressor map and the training data to represent the compressor power in the entire operating range of the compressor forms the uncertainty from model random error.

There are other sources of uncertainties that are neglected in this study. For example, although the uncertainty due to numerical approximation exists because of the numerical procedure used in the calculation of the compressor map, they are assumed to be negligible because the solution of the polynomial is explicit and is not complex. Uncertainties due to manufacturing tolerances, aging, and wear are also neglected in the current work because data on these issues in public literature is limited.

The combination of the four remaining major uncertainty components - uncertainty due to inputs, uncertainty due to training data, uncertainty due to outputs, and uncertainty due to model random error - creates the overall standard uncertainty of the compressor map output, which can be expanded to the overall expanded uncertainty by defining a confidence level as suggested in ASME Performance Test Codes (PTC) 19.1-2013 (ASME 2013).

Uncertainty of pressure measurement

Uncertainty of pressure measurement ΔP_{mea} is usually described as a percentage r_p of full scale measurement P_{full} in the specification of a pressure transducer. It can be calculated by Eq. (8).

$$\Delta P_{mea} = r_P P_{full} \tag{8}$$

For uncertainties that are decscribed as the percentage of measured pressure r_{mea}, Eq. (9) can be used

.

$$\Delta P_{mea} = r_{mea} P_{mea} \qquad (9)$$

Uncertainty due to equation of state

Uncertainty of equation of states is the uncertainty of the estimation equation of dew point temperature from pressure, and it differs between equations of states. Its values for different refrigerants are tabulated in Table 1.

Table 1: Uncertainty of equations of states of different refrigerant		
Refrigerant	Uncertainty	Literature
R22	0.2% of the dew point pressure	Kamei et al. (1995)
R404A	0.5% of the dew point pressure	Lemmon (2003)
R410A	0.5% of the dew point pressure	Lemmon (2003)

The uncertainty of dew point pressure due to the equation of states can be expressed by Eq. (10).

$$\Delta P_{EOS} = r_{EOS} P_{mea} \qquad (10)$$

Uncertainty of dew point temperature

The uncertainty of dew point temperature is formed by combining the uncertainty of pressure measurement and uncertainty due to equation of state. Assuming that the two uncertainties are not correlated, the low-order uncertainty of dew point temperature can be computed by Eq. (11) according to Joint Committee for Guides in Metrology (JCGM) Guide to the Expression of Uncertainty Measurement (GUM) 100-2008 (JCGM 2008).

$$\Delta T_{dew,low} = \sqrt{\left(\frac{\partial T_{dew}(P_{mea})}{\partial P}\right)^2 \cdot (\Delta P_{mea}^2 + \Delta P_{EOS}^2)} \qquad (11)$$

The high-order uncertainty can be calculated by Eq. (12) following the same standard.

$$\Delta T_{dew,high} = \sqrt{\frac{1}{2}\left(\frac{\partial^2 T_{dew}(P_{mea})}{\partial P^2}\right)^2 \cdot (\Delta P_{mea}^4 + \Delta P_{EOS}^4)} \qquad (12)$$

Although JCGM GUM 100-2008 recommends the use of third-order partial derivatives to calculate the high-order uncertainty, they are difficult to be calculated for equation of states and are assumed to be negligible in this paper.

The partial derivatives in Eq. (11) and (12) are calculated by the method in Thorade and Saadat (2013), and the calculation is implemented by the software CoolProp (Bell et al. 2014). The overall standard uncertainty of the dew point temperature is the sum of squares of the uncertainty component in Eq. (11) and (12) as shown in Eq. (13).

$$\Delta T_{dew} = \sqrt{\Delta T_{dew,low}^2 + \Delta T_{dew,high}^2} \tag{13}$$

Uncertainty due to inputs

Uncertainties of inputs to the compressor map - compressor suction and discharge dew point temperature - propagate to the map output and form the uncertainty due to inputs. According to the Joint Committee for Guides in Metrology (JCGM) Guide to the Expression of Uncertainty Measurement (GUM) 100-2008 (JCGM 2008), the low-order uncertainty due to inputs can be calculated by Eq. (14).

$$\Delta \widehat{W}_{comp,input,low} = \sqrt{\left(\frac{\partial \widehat{W}_{comp}}{\partial T_{dew,suc}}\right)^2 \Delta T_{dew,suc}^2 + \left(\frac{\partial \widehat{W}_{comp}}{\partial T_{dew,dis}}\right)^2 \Delta T_{dew,dis}^2} \tag{14}$$

The low-order uncertainty in Eq. (14) calculates the uncertainty due to inputs accurately if the map is linear and hence a first-order polynomial. However, compressor map is a cubic and a high-order polynomial. According to the JCGM GUM 100-2008, there may be a significant uncertainty component as a result of the high-order terms. The component is labeled as high-order uncertainty due to inputs and is calculated by Eq. (15).

$$\Delta \widehat{W}_{comp,input,high} = \sqrt{\begin{aligned} &\left(\left(\frac{\partial^2 \widehat{W}_{comp}}{\partial T_{dew,suc} \partial T_{dew,dis}}\right)^2 + \frac{\partial \widehat{W}_{comp}}{\partial T_{dew,suc}} \frac{\partial^3 \widehat{W}_{comp}}{\partial T_{dew,suc} \partial T_{dew,dis}^2}\right. \\ &\left. + \frac{\partial \widehat{W}_{comp}}{\partial T_{dew,dis}} \frac{\partial^3 \widehat{W}_{comp}}{\partial T_{dew,suc}^2 \partial T_{dew,dis}}\right) \Delta T_{dew,suc}^2 \Delta T_{dew,dis}^2 \\ &+ \left(\frac{1}{2}\left(\frac{\partial^2 \widehat{W}_{comp}}{\partial T_{dew,suc}^2}\right)^2 + \frac{\partial \widehat{W}_{comp}}{\partial T_{dew,suc}} \frac{\partial^3 \widehat{W}_{comp}}{\partial T_{dew,suc}^3}\right) \Delta T_{dew,suc}^4 \\ &+ \left(\frac{1}{2}\left(\frac{\partial^2 \widehat{W}_{comp}}{\partial T_{dew,dis}^2}\right)^2 + \frac{\partial \widehat{W}_{comp}}{\partial T_{dew,dis}} \frac{\partial^3 \widehat{W}_{comp}}{\partial T_{dew,dis}^3}\right) \Delta T_{dew,dis}^4 \end{aligned}} \tag{15}$$

The partial derivatives in Eq. (14) and (15) are calculated analytically by taking the partial derivative of the compressor map with respect to the compressor suction and discharge dew point temperature.

The uncertainty due to inputs is the sum of the low-order and high-order uncertainties and can be calculated by Eq. (16).

$$\Delta \widehat{W}_{comp,input} = \sqrt{\Delta \widehat{W}_{comp,input,low}^2 + \Delta \widehat{W}_{comp,input,high}^2} \tag{16}$$

The low-order uncertainty due to inputs without the uncertainty due to the equation of state is usually the only uncertainty computed as the uncertainty of the compressor map.

Uncertainty due to training data

Uncertainty due to training data is the uncertainty component caused by the propagation of uncertainty of training data to the regression coefficients in the compressor map. According to Cheung and Bach (2015), the uncertainty component, assuming all training data to be uncorrelated, can be calculated by Eq. (17).

$$\Delta \dot{W}_{comp,train,uncorr} = \sqrt{ \begin{array}{l} \sum_{j=1}^{n} \left(\sum_{i=1}^{m} \left(\dfrac{\partial \widehat{W}_{comp}}{\partial \beta_i} \dfrac{\partial \beta_i}{\partial T_{dew,suc,train,j}} \right) \Delta T_{dew,suc,train,j} \right)^2 \\ + \sum_{j=1}^{n} \left(\sum_{i=1}^{m} \left(\dfrac{\partial \widehat{W}_{comp}}{\partial \beta_i} \dfrac{\partial \beta_i}{\partial T_{dew,dis,train,j}} \right) \Delta T_{dew,dis,train,j} \right)^2 \\ + \sum_{j=1}^{n} \left(\sum_{i=1}^{m} \left(\dfrac{\partial \widehat{W}_{comp}}{\partial \beta_i} \dfrac{\partial \beta_i}{\partial \dot{W}_{comp,train,j}} \right) \Delta \dot{W}_{comp,train,j} \right)^2 \end{array} } \tag{17}$$

However, Eq. (17) does not consider the correlation effect between data points in the training data. In the training data, all compressor suction dew point temperatures come from the same pressure transducer at the compressor suction. This means that the uncertainties of all compressor suction dew point temperature in the training data are correlated because they are measured by the same sensors and hence sensors with the same calibration reference, and the propagation of uncertainties from the compressor suction dew point temperatures should account for the correlation. This means that another uncertainty component is needed to calculate the uncertainty due to correlation of training data. By following the procedure in ASME PTC 19.1-2013 (ASME 2013) and considering the compressor discharge dew point temperature and power consumption similarly, the uncertainty due to correlated training data is given as Eq. (18).

$$\Delta \dot{W}_{comp,train,corr} = \sqrt{\begin{array}{l} 2\sum_{j=1}^{n-1}\sum_{k=j+1}^{n}\left(\begin{array}{l} \sum_{i=1}^{m}\left(\dfrac{\partial \widehat{W}_{comp}}{\partial \hat{\beta}_i}\dfrac{\partial \hat{\beta}_i}{\partial T_{dew,suc,train,j}}\right)\Delta T_{dew,suc,train,j} \cdot \\ \left(\dfrac{\partial \widehat{W}_{comp}}{\partial \hat{\beta}_i}\dfrac{\partial \hat{\beta}_i}{\partial T_{dew,suc,train,k}}\right)\Delta T_{dew,suc,train,k} \end{array}\right) \\ +2\sum_{j=1}^{n-1}\sum_{k=j+1}^{n}\left(\begin{array}{l} \sum_{i=1}^{m}\left(\dfrac{\partial \widehat{W}_{comp}}{\partial \hat{\beta}_i}\dfrac{\partial \hat{\beta}_i}{\partial T_{dew,dis,train,j}}\right)\Delta T_{dew,dis,train,j} \cdot \\ \left(\dfrac{\partial \widehat{W}_{comp}}{\partial \hat{\beta}_i}\dfrac{\partial \hat{\beta}_i}{\partial T_{dew,dis,train,k}}\right)\Delta T_{dew,dis,train,k} \end{array}\right) \\ +2\sum_{j=1}^{n-1}\sum_{k=j+1}^{n}\left(\begin{array}{l} \sum_{i=1}^{m}\left(\dfrac{\partial \widehat{W}_{comp}}{\partial \hat{\beta}_i}\dfrac{\partial \hat{\beta}_i}{\partial \dot{W}_{comp,train,j}}\right)\Delta \dot{W}_{comp,train,j} \cdot \\ \left(\dfrac{\partial \widehat{W}_{comp}}{\partial \hat{\beta}_i}\dfrac{\partial \hat{\beta}_i}{\partial \dot{W}_{comp,train,k}}\right)\Delta \dot{W}_{comp,train,k} \end{array}\right) \end{array}} \tag{18}$$

With the absence of squared terms in Eq. (18), the uncertainty due to correlated training data can be a complex number, unlike other uncertainty components which are real and positive.

All partial derivatives in Eq. (17) and (18) are calculated analytically, and the details of the analytical partial derivatives of coefficients with respect to training data points are listed in the Appendix A for reference.

The overall uncertainty due to training data is calculated by Eq. (19).

$$\Delta \widehat{W}_{comp,train} = \sqrt{\Delta \widehat{W}_{comp,train,uncorr}^2 + \Delta \widehat{W}_{comp,train,corr}^2} \tag{19}$$

Uncertainty due to model random error

The linear regression equation contains an error due to the insufficiency of the model to represent the mathematical surface of the model output completely (ε in Eq. (1)), and linear regression assumes that the error is normally distributed around zero with some finite variance. Unlike the aforementioned uncertainty due to training data which is zero if all training data are measured with zero uncertainty, ε (as defined in equation 1) is finite as far as there is a difference between the model result and the corresponding measurment in the training data. This is possible if the model under consideration does not account for all effects comprehensively (e.g. change of surrounding temperature around the compressor and hence compressor heat loss), and its contribution to the uncertainty of the map should be accounted for in addition

to the uncertainty due to training data. Statistical textbooks (e.g. Montgomery 2005) illustrate that the error can be approximated with the expression in Eq. (20).

$$\Delta \widehat{W}_{comp,model} = \sigma \sqrt{1 + \vec{x}^T (X_{train}^T X_{train})^{-1} \vec{x}}, \tag{20}$$

where the mean square error σ in Eq. (20) can be calculated by Eq. (21).

$$\sigma = \sqrt{\frac{\sum_{i=1}^{n}(y_{train,i} - \vec{x}^T \hat{\vec{\beta}})^2}{n - m}} \tag{21}$$

Eq. (20) gives the uncertainty due to model random error, and this is also the prediction uncertainty with error in the predictor variables and the model coefficients as specified in the *Informative Annex A* in ASHRAE Guideline 2–2010 (ASHRAE 2010a).

Roy and Oberkampf (2011) describe a method using validation metric to obtain the uncertainty due to model random error by extra experimental observations. However, the method needs extra experimental observations and is not used in this paper. There are also other types of models with a different true equation as Eq. (1) such as Ruch et al. (1993) that accounts for correlation between temperature data and time and the Bayesian calibration method in Kennedy and O'Hagan (2001) that considers user-defined probability distributions of coefficients and tunes the distributions according to the training data for the estimation of coefficients. Their uncertainties from model random error in these models will be calculated with other forms of equations.

Uncertainty due to output

Uncertainty of compressor map output should represent the probable difference between the true value and the model output. However, because the map is trained by measured compressor power consumption, the summation of uncertainty components of compressor map output from other sources would only represent the probable difference between the estimated and measured value of the compressor power consumption. To correctly represent the uncertainty, another component of uncertainty must be added. This is the uncertainty due to outputs and can be approximated by Eq. (22).

$$\Delta \widehat{W}_{comp,output} = \frac{\widehat{W}_{comp}}{n} \sum_{i=1}^{n} \frac{\Delta W_{train,i}}{W_{train,i}} \tag{22}$$

Eq. (22) is only applicable to regression models with a normally distributed error term defined in the same way as Eq. (1). If the error term is defined differently like the error term that is dependent on the input variables as the one in Kennedy and O'Hagan (2001), then Eq. (22) will not be applicable to the regression model.

Other negligible uncertainties

One of the uncertainties to be neglected is uncertainty due to numerical approximation. Roy and Oberkampf (2011) describe three sources of uncertainty due to numerical approximation: uncertainty due to discretization, uncertainty due to incomplete iteration and uncertainty due to computational round off that are all results. Because linear regression does not involve discretization and iterative calculation and the computation involves 16 significant figures, the uncertainty due to numerical approximation in the compressor map output can be assumed to be negligible.

Other systematic uncertainties due to conceptual errors in Moffat (1988) are also neglected in this study. Their magnitude varies dramatically depending on the causes of the error, and examples include uncertainties due to manufacturing process, system or sensor ageing, and sensor installation location. If it is caused by a small change of sensor installation location by a model user, it can be negligible. However, if it is caused by significant ignorance of a model user such as using the compressor suction temperature instead of compressor suction saturation temperature at the input of the compressor map, they can become more significant than the uncertainties discussed in this manuscript. Although they can be the largest among all uncertainties according to Moffat (1988), they are neglected because of the lack of data to estimate them and they are only significant due to defects or model user ignorance that is too subjective to be quantified (e.g. application of models under conditions they were not developed for). Uncertainties due to manufacturing and ageing are created when a map output is used to estimate the power consumption of a compressor of the same model but in a different setup at a different point of usable lifetime. Because its quantification can only be done by testing multiple compressors of the same model from a production line with a well-balanced test matrix and some design of experiments methods, it is assumed to be negligible in this study for simplicity. However, if a model of compressor is not produced with consistent quality, this uncertainty will become significant and should be taken into account for correct uncertainty calculation.

Likewise, uncertainty due to sensor installation location is created if the inputs are taken from sensors that are installed differently than the sensors used to collect the training data. While they are often small, incorrect sensor installation may increase this uncertainty significantly.

Overall standard uncertainty

Because the uncertainty components are not correlated with each other, the overall standard uncertainty of the compressor map output can be calculated by the sum of squares of the uncertainty components as shown in Eq. (23).

$$\Delta \widehat{W}_{comp,std} = \sqrt{\Delta \widehat{W}_{comp,input}^2 + \Delta \widehat{W}_{comp,train}^2 + \Delta \widehat{W}_{comp,model}^2 + \Delta \widehat{W}_{comp,output}^2} \tag{23}$$

Overall expanded uncertainty

According to ASME PTC 19.1-2013, the standard uncertainty is multiplied by a coverage factor to illustrate the level of confidence and the accepted practice uses a 95% level of confidence. Because the number of training data points of the compressor map may be smaller than 60 in this study, the Student's t value of the Student's t distribution is used to calculate the expanded uncertainty as shown in Eq. (24).

$$\Delta \widehat{W}_{comp,exp} = t_{n-m,0.95} \cdot \Delta \widehat{W}_{comp,std} \tag{24}$$

Case Study

To examine if the method can calculate extrapolation uncertainties of compressor maps appropriately, compressor calorimeter testing data from Shrestha et al. (2013a) and Shrestha et al. (2013b) are used. The tests were done to compare the performance of compressors using different refrigerants. Because this method uses uncertainty of equation of state, only compressor data using refrigerants with well-defined equations of state are considered in this study. The specifications of the compressors are listed in Table 2.

Table 2: Specification of compressors		
Specification	**Compressor 1 (Shrestha et al. 2013a)**	**Compressor 2 (Shrestha et al. 2013b)**
Compressor type	Hermetic scroll	
Frequency [Hz]	60	
Voltage [V]	208/230	

Displacement volume [cm^3 rev^{-1}]	20.3	51.0
Refrigerant	R410A	R404A
Rated power consumption [W]	2170	3320
Superheat [K]	11.1	

The compressors were tested in calorimeters following the ANSI/ASHRAE Standard 23.1-2010 (ASHRAE 2010b). The uncertainties and locations of the sensors used in the setup are tabulated in Table 3.

Table 3: Uncertainties of sensors used in the setup			
Sensors	**Locations**	**Measurement range**	**Uncertainty**
Power energy meter	Compressor power consumption	Not available from the data source	±0.5% of the measured value
Pressure transmitter 1	Compressor discharge	0 – 5170 kPa	±0.25% full scale
Pressure transmitter 2	Compressor suction	0 – 1380 kPa	±0.25% full scale
Refrigerant mass flowmeter	Condenser outlet	Not available from the data source	±0.10% of the measured value

Each compressor was tested under a variety of conditions. To analyze how different sets of training data affect the size of extrapolation uncertainty, each data set of compressor data is divided into 3 subsets. The operating conditions of the testing data and the subsets are shown in Figure 2.
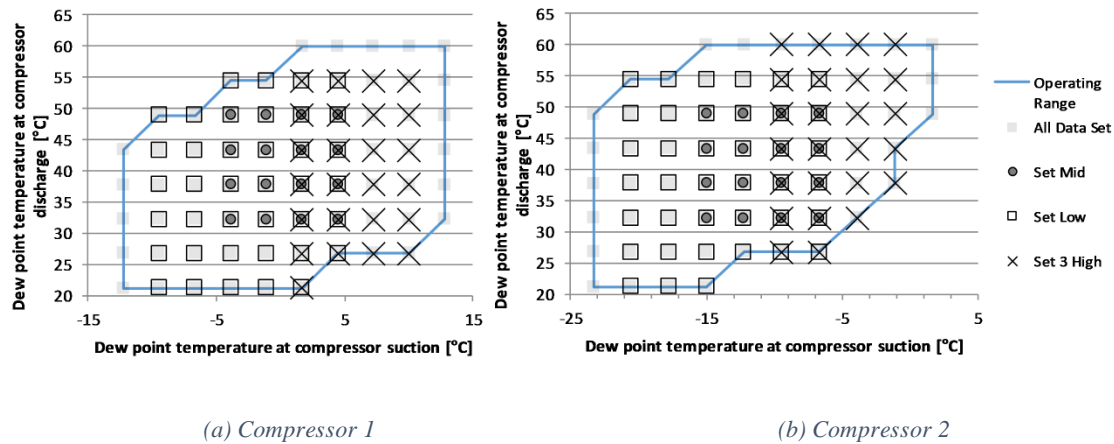
(a) Compressor 1   *(b) Compressor 2*

Figure 2: Operating conditions in compressors tests and the subsets defined for extrapolation uncertainty studies

Figure 2 shows the range of all testing conditions and the subsets for each compressor. Compressor 1 data has 66 available points with compressor discharge dew point temperature ranging from 21.1℃ to 60℃ and compressor suction dew point temperature ranging from -12.2℃ to 12.8℃. Compressor 2 data has 63 available points with compressor discharge dew point temperature ranging from 21.1℃ to 60℃ and compressor suction dew point temperature ranging from -23.3℃ to 1.67℃. All Data Set in Figure 2 consists of all testing data points. Set Mid is designed to include data points at the center of the operating range only, Set Low is designed to include data points with lower dew point temperatures relative to the

operating range only, and Set High is designed to include data points with high compressor suction dew point temperature only.

The choice of training data in Figure 2 is arbitrary in order to demonstrate how the uncertainty quantifies the effect of extrapolation on the model. In reality, compressor maps are created with at least 14 data points scattered across the entire operating range as shown in Aute et al. (2015), and techniques in design of experiments such as Latin-Hypercube-Sampling or D-optimality may be used to choose the appropriate data points (Montgomery 2005).

The sets of each compressor are used to train their compressor maps separately, and their map outputs and map output uncertainties of all data points are calculated and compared in the next section.

Although it can be easily observed if a data point lies outside a set and if its corresponding estimation extrapolates from a map in Figure 2, it is necessary to define a metric for the degree of extrapolation to analyze the results from all 8 compressor maps. In this case study, the normalized degree of extrapolation is quantified by Eq. (25).

Normalized degree of extrapolation (25)

$$= \sqrt{\left(\frac{T_{dew,suc} - T_{dew,suc,close}}{T_{dew,suc,train,max} - T_{dew,suc,train,min}}\right)^2 + \left(\frac{T_{dew,dis} - T_{dew,dis,close}}{T_{dew,dis,train,max} - T_{dew,dis,train,min}}\right)^2}$$

Eq. (25) shows an equation to calculate the normalized degree of extrapolation which is the normalization of the shortest distance of an operating point on the boundary of the training data of a map in Figure 2. While the equation is intuitive to solve for an operating range with a well-defined boundary as shown in Figure 2, the operating conditions of some compressor maps may not align with the compressor testing data as regularly as Figure 2 and the compressor operating range may not be as rectangular as Figure 2 (Winandy et al. 2002; Jähnig et al. 2002). The equation will hence become difficult to be solved in those situations.

In addition to Eq. (25), a few metrics are needed to summarize the accuracy and uncertainty of the map results. To summarize the accuracy of the maps, the coefficient of variation from ASHRAE Guideline 14-2014 (ASHRAE 2014) to assess building model accuracy is used. Its calculation is illustrated in Eq. (26), and a smaller value implies a more accurate model.

$$COV = \frac{\text{Sample standard deviation}}{\text{Mean of the map outputs}} = \frac{n\sqrt{\sum_{i=1}^{n}(\widehat{W}_{comp,i} - W_{comp})^2}}{\sqrt{n-1}\sum_{i=1}^{n}\dot{W}_{comp,i}} \qquad (26)$$

The other metric is relative uncertainty which compares the magnitude of the uncertainty with the map outputs, and a larger relative uncertainty implies that the value of the map output may deviate more with its true value. Relative uncertainty is calculated per Eq. (27).

$$\text{Relative overall uncertainty} = \frac{\Delta\widehat{W}_{comp,exp}}{\widehat{W}_{comp}} \qquad (27)$$

Similarly, a relative uncertainty of an uncertainty component as calculated in Eq. (28) is used.

$$\text{Relative uncertainty of an uncertainty component} = \frac{\Delta\widehat{W}_{comp,decoupled}}{\widehat{W}_{comp}} \qquad (28)$$

where $\Delta\widehat{W}_{comp,decoupled}$ in Eq. (28) can be any uncertainty component.

Results and Discussion

Accuracy of maps and example application of the method

To examine the accuracy of the maps within the training data points, the coefficients of variation of different maps calculated from their estimation over their training data points are tabulated in Table 4.

Table 4: Coefficients of variation over their training data points for all trained compressor maps					
Compressor 1	**Coefficient of variation**	**Number of training data points**	**Compressor 2**	**Coefficient of variation**	**Number of training data points**
Map from All Data Set	0.0021	66	Map from All Data Set	0.0013	63
Map from Set Mid	0.0004	16	Map from Set Mid	0.0002	16
Map from Set Low	0.0021	39	Map from Set Low	0.0012	39
Map from Set High	0.0010	25	Map from Set High	0.0007	25

Table 4 shows that the coefficients of variation for all maps over their training data points are smaller than 1%, and hence the maps should be very accurate over the range of their training data points. However, the maps may not be accurate when extrapolated. To illustrate the potential inaccuracy, the estimated power consumption of map from Set High of both compressors is plotted in Figure 3.
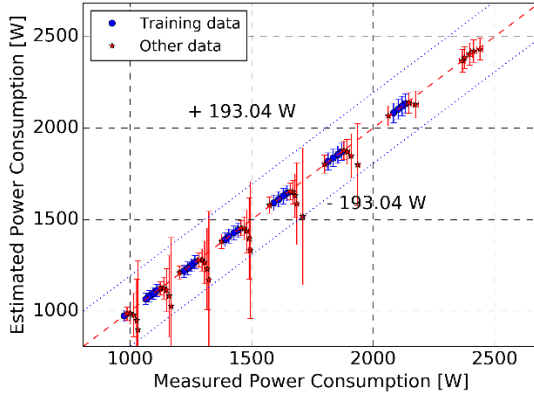
(a) Compressor 1   *(b) Compressor 2*
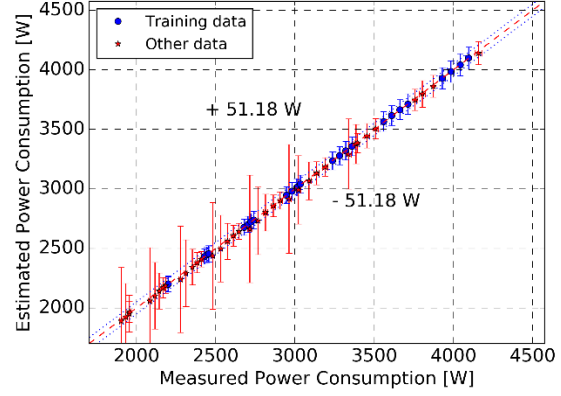
Figure 3: Comparison between measured and estimated power consumption for the map from Set High of both compressors with overall expanded uncertainty of map outputs

Figure 3 shows that maps from Set High of both compressor's maps are able to estimate the power consumption at the conditions of training data points correctly. However, when the uncertainty of the estimation is high at conditions different from the training data, the map from Set High of compressor 1 cannot predict the power consumption accurately while the map from Set High of compressor 2 can predict accurately.

Figure 3 also demonstrates an example application of the uncertainty calculation method. In Figure 3(a), some data points are estimated with small uncertainty values and high accuracy despite their absence in the training data. This shows that the estimation of power consumption at these data points can be trusted and used for other purposes. However, the ones with large uncertainties are also associated with high inaccuracy, indicating that they cannot be trusted unless training data at conditions other that the Set High in Figure 2 are introduced. Although the rule is not well followed by the results in Figure 3(b), this is true for other choices of sets as shown in the Appendix B, indicating that the uncertainty calculation method can be used to identify if the estimation of power consumption under certain condition is reliable and can be trusted according to its training data conditions.

Change of overall expanded uncertainty with degree of extrapolation

In order to analyze if the overall expanded uncertainty can represent the degree of extrapolation at a data point, the normalized degrees of extrapolation from Eq. (25) is plotted with the relative overall uncertainty for all maps defined in Figure 2 as shown in Figure 4.
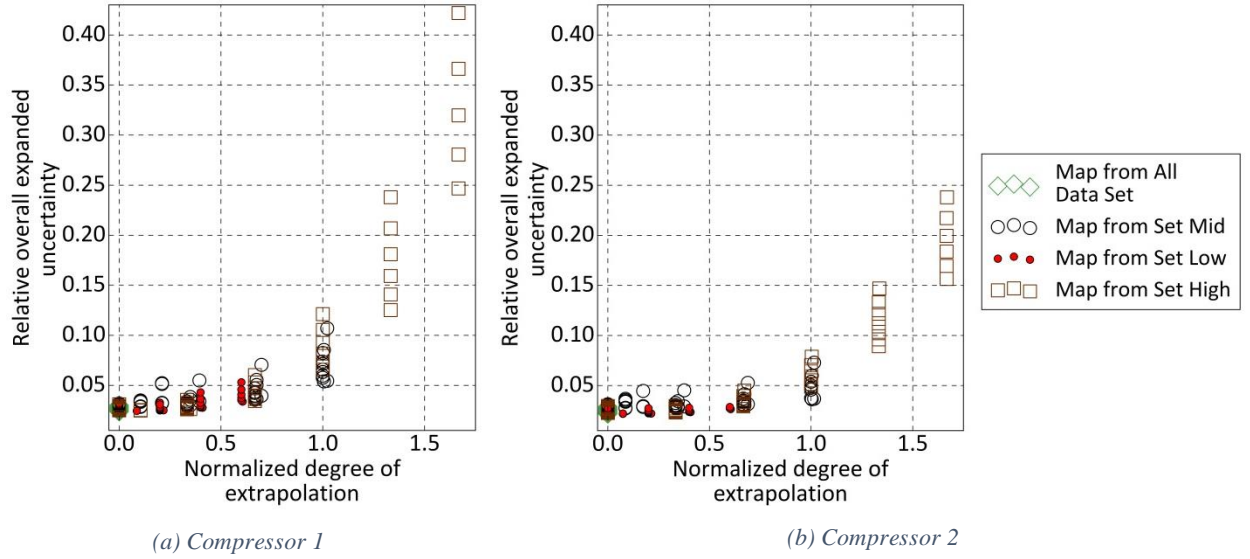
(a) Compressor 1

(b) Compressor 2

Figure 4: Change of relative overall expanded uncertainty with normalized degree of extrapolation for all maps

Figure 4 shows that for maps in both compressors, the relative overall uncertainty depends strongly on the normalized degree of extrapolation and increases with an increase in the normalized degree of extrapolation. A similar behavior was observed in Cheung and Bach (2015) for an increase in extrapolation, there expressed in terms of minimum ℃ distance to nearest training data point.

Change of overall expanded uncertainty with map accuracy

Figure 5 is plotted to understand how the uncertainty changes with map accuracy.

(a) Compressor 1　　　　　*(b) Compressor 2*
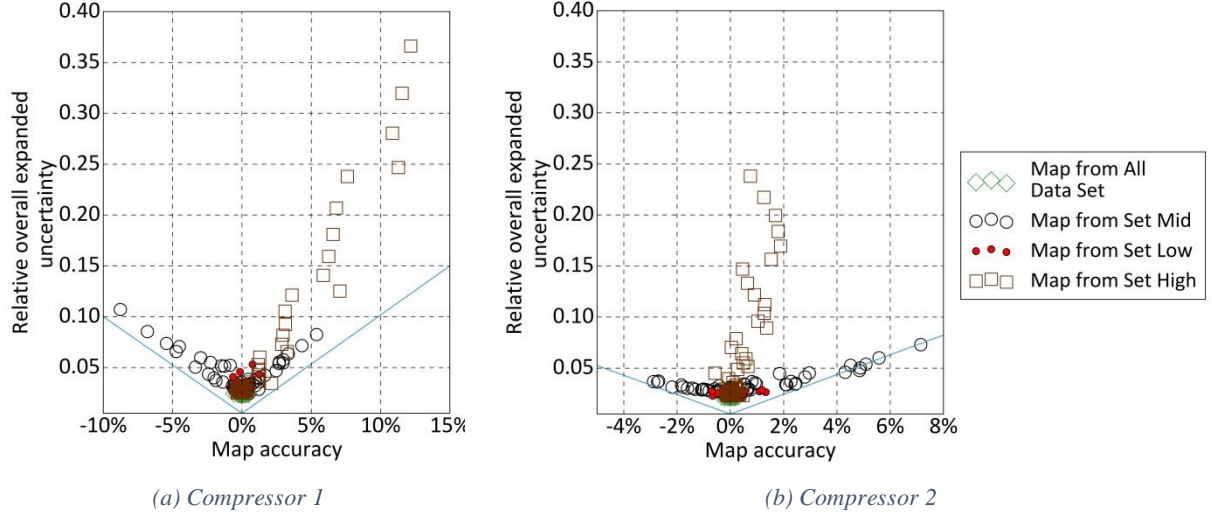
Figure 5: Change of relative overall expanded uncertainty with map accuracy in all maps

Figure 5(a) for compressor 1 shows that the accurate maps have low relative uncertainty and uncertainty increases with an increase in map inaccuracy as found in Cheung and Bach (2015). For compressor 2, Figure 5(b) shows that maps from Set Mid and Low show the similar behavior as maps in compressor 1, however, map from Set High has almost same accuracy for different values of overall relative uncertainty. This shows that the map accuracy does not have a definite relationship with relative overall uncertainty and maps that are accurate at extrapolation may still yield large relative overall uncertainty.

Figure 5 also shows an approach for a user to justify the use of an extrapolation scenario based on the overall expanded uncertainty. A user can use the maximum relative overall expanded uncertainties at the training data points to set a threshold, and reject any extrapolation cases with overall expanded uncertainty is higher than that threshold. For example, the maximum relative overall expanded uncertainty at the training data points of the map generated from Set Mid of Compressor 2 is 0.0313. If a user uses the map to estimate the power consumption of all Compressor 2 data points in Figure 2(b) and rejects cases with relative overall uncertainties higher than 0.0313, the user can keep 19 out of 47 extrapolation cases with an average map accuracy at 0.75% among the accepted extrapolation cases and achieves a good accuracy relative to the average map accuracy at 0.44% for the training data points. If a user can tolerate higher inaccuracy at the extrapolation cases, a threshold higher than the maxmium value can be set to match the needs of different users.

Change of uncertainty components with extrapolation

To find the uncertainty component that increases with extrapolation, the squares of uncertainty components of map outputs in all maps are plotted with the normalized degree of extrapolation as shown in Figure 6.
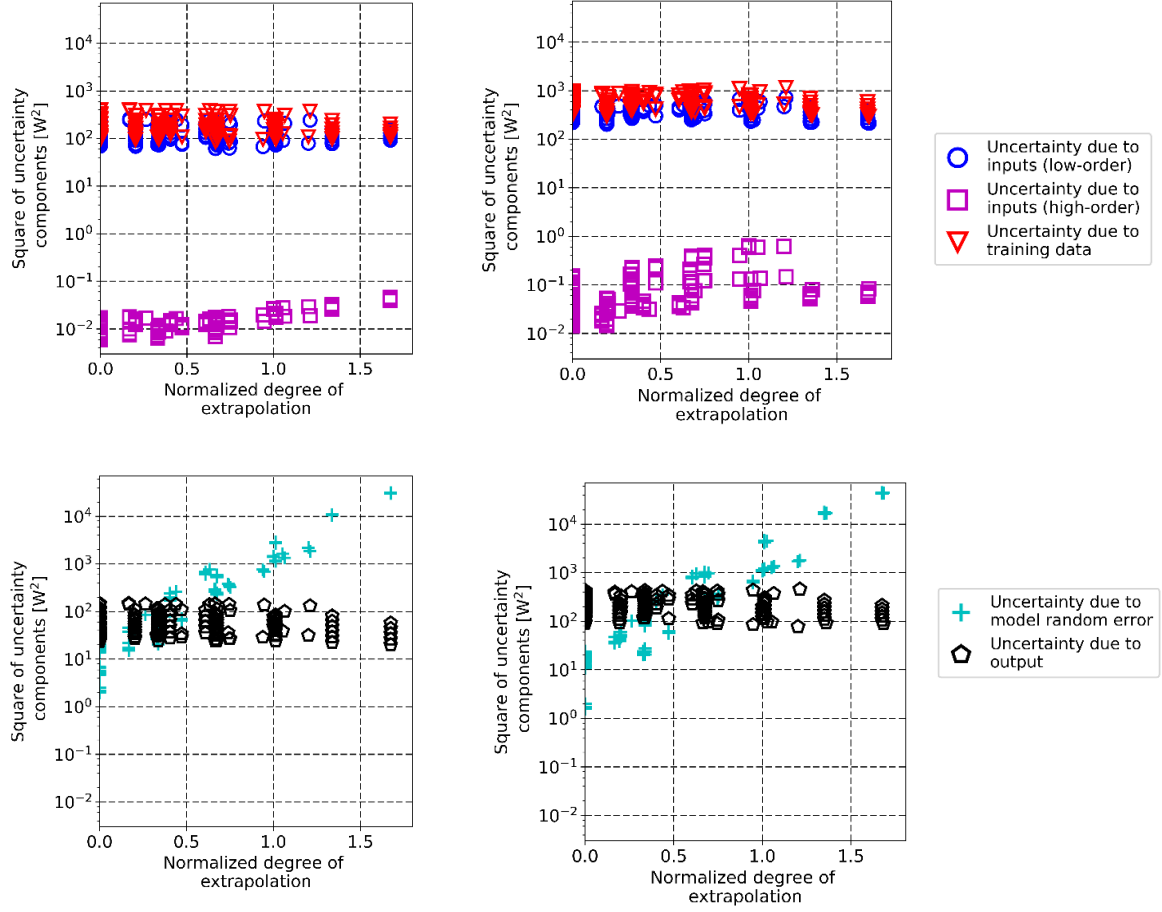
(a) Compressor 1

(b) Compressor 2

Figure 6: Change of uncertainty components in map outputs with normalized degree of extrapolation in all maps

The uncertainty components in Figure 6 are squared because uncertainty due to correlated training data can be complex. It shows that the uncertainty due to model random error increases as normalized degree of extrapolation increases. This shows that the uncertainty due to model random error is responsible for the increase of the uncertainty as the compressor maps extrapolate. The significance of other uncertainty components remains the same with extrapolation, and it can be listed in a descending order as the

uncertainty due to training data, the low-order uncertainty due to inputs, the uncertainty due to output and the high-order uncertainty due to inputs, which is insignificant and can be neglected.

The results in Figure 6 also show that the calculation method is different from that in Aute et al. (2015) because their method, as shown by Coleman and Steele (2009) to be equivalent to the uncertainty due to inputs and uncertainty due to training data, would under-predict the uncertainty when the degree of extrapolation is higher than 1.0 and the uncertainty due to model random error is significant. Hence the method presented in this paper will lead to better predictions than the method presented by Aute et al. (2015) when extrapolation occurs.

One major difference between Figure 6 and the conclusion in Cheung and Bach (2015) is that the uncertainty due to training data in Figure 6 does not increase with extrapolation unlike the conclusion in Cheung and Bach (2015). The reason is that Cheung and Bach (2015) does not include the uncertainty due to correlated training data as calculated in Eq. (18).
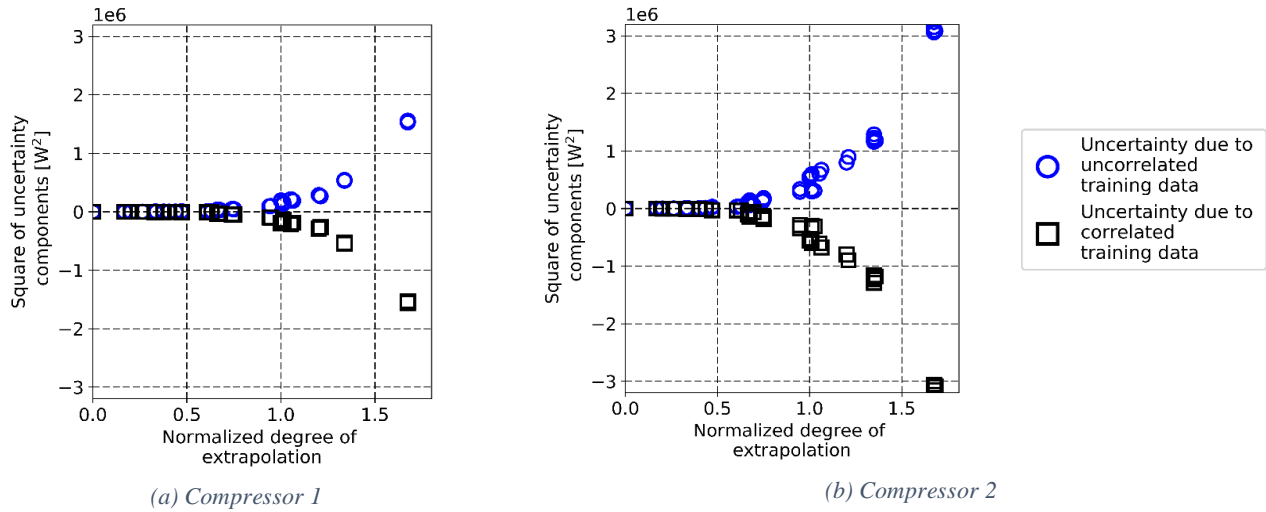
(a) Compressor 1   *(b) Compressor 2*

Figure 7: Change of components of uncertainty due to training data in map outputs with normalized degree of extrapolation in all maps

Figure 7 shows that the uncertainty due to uncorrelated training data increases with extrapolation as found in Cheung and Bach (2015). However, the correlation of training data that is decreasing with extrapolation in Figure 7 is not considered in Cheung and Bach (2015). Unlike other uncertainty components, the square of the uncertainty due to correlated training data can be negative because all of its terms in Eq. (18) are not restricted to be positive. As maps extrapolate, the reduction of the uncertainty of

correlated data partially offsets the increase of the uncertainties of the uncorrelated data, resulting in relatively constant uncertainty due to training data in Figure 6. Hence the uncertainty due to correlated training data is not negligible if uncertainty due to training data is calculated.

Change of uncertainty due to training data with choice of training data

To examine the choices of training data affect uncertainty due to training data, the relative uncertainties from training data of different maps are compared with each other as shown in Figure 8.
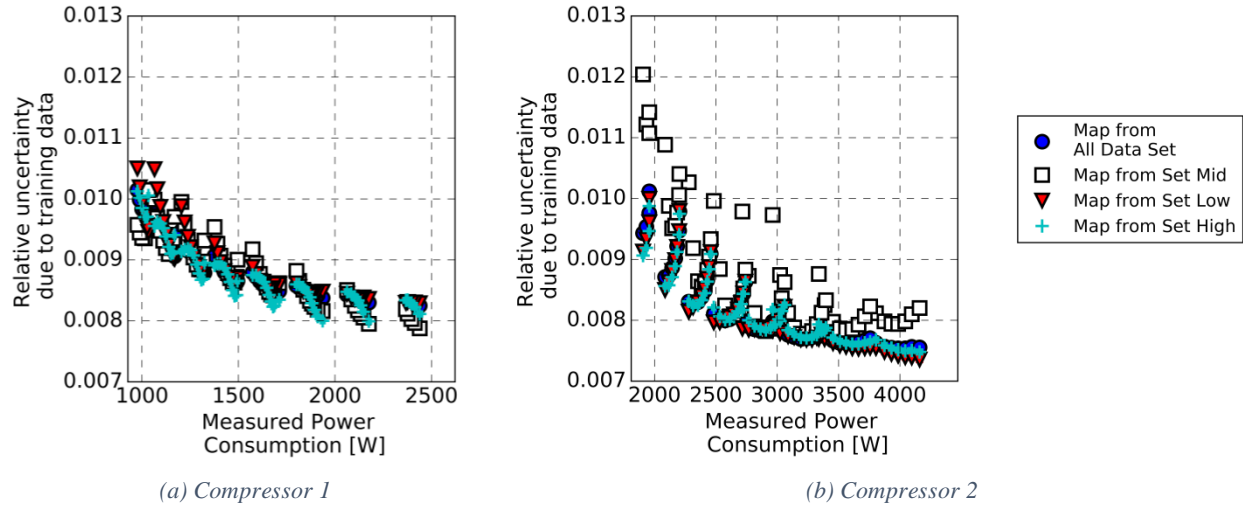
(a) Compressor 1   *(b) Compressor 2*

Figure 8: Comparison of uncertainties due to training data from different maps at all operating conditions

Figure 8 shows that the uncertainties due to training data from different maps are not significantly different for both compressors and all of them decrease with higher compressor power consumption. This shows that the magnitude of uncertainty due to training data does not depend on the choice of training data of compressor maps but on other factors such as the input conditions of the compressor or the magnitude of the training data.

Application of the method to other types of compressor map outputs

The 10-coefficient map in Eq. (6) is not only applied to power consumption estimation but also to other variables of compressors such as refrigerant mass flow rate and cooling capacity of a vapor compression system. To examine if the uncertainty calculation method is applicable to other types of outputs, the method is applied to the refrigerant mass flow rates measured in Shrestha et al. (2013a) and Shrestha et al. (2013b) in a similar manner, and the results are shown in Figure 9 and Figure 10.
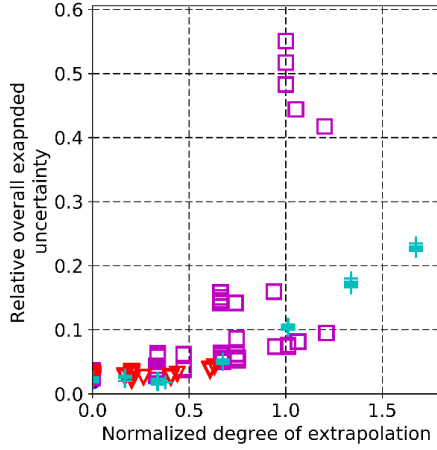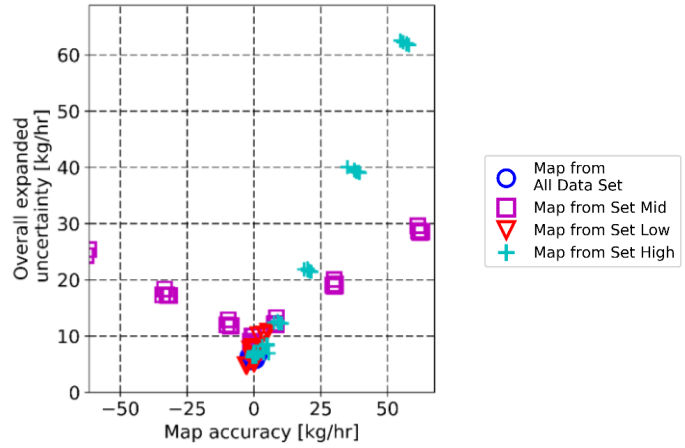
(a) Compressor 1
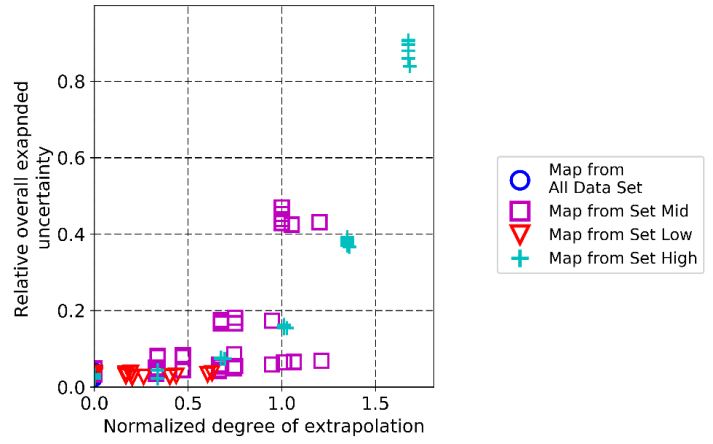
(b) Compressor 2

Figure 9: Change of relative overall expanded uncertainty with normalized degree of extrapolation for all maps estimating refrigerant mass flow rates
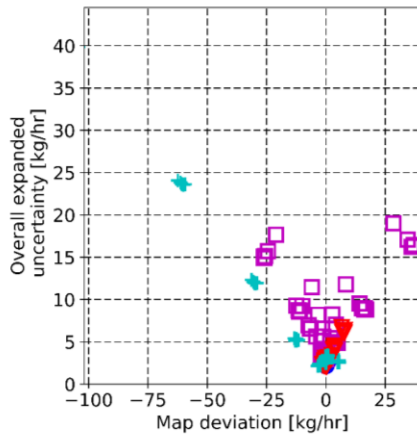
(a) Compressor 1

(b) Compressor 2

Figure 10: Change of overall expanded uncertainty with map deviation in all maps estimating refrigerant mass flow rate

Figure 9 and Figure 10 show similar results as the power consumption compressor maps. Extrapolation cases show high overall expanded uncertainties and high overall expanded uncertainties refer to cases with poor map accuracy. Hence the method is also applicable to other types of compressor maps.

Conclusions and future work

In summary, a method to calculate the uncertainty of compressor map output is developed. The method considers the effects of the mathematical structure of the map, the choice of training data, the uncertainties

of the training data, the uncertainties of related measurement devices, and the equation of state of refrigerants. It calculates the map output uncertainty by 4 major components and is tested with case studies by measurement data from 2 compressors. The results show that high-order uncertainties are negligible despite the cubic structure of the map. With little extrapolation, the uncertainty due to training data is the most significant uncertainty component though uncertainty due to inputs is the most common one to be calculated. When the maps extrapolate, their uncertainties due to model random error increases with map extrapolation and may become larger than other components. Although the uncertainty due to model random error is a good indicator of extrapolation inaccuracy, extrapolation may not necessarily imply inaccuracy of the maps and hence the method occasionally exaggerates the inaccuracy problem due to extrapolation, which would require future work for improvement. By calculating the overall expanded uncertainty of a compressor map and defining an accuracy threshold, a user can decide if an extrapolation case is acceptable. The method allows the quantification of the extrapolation effect of the compressor model and helps to verify thermal system models that simulate off-design conditions (ASME 2006; Coleman and Steele 2009). Such conditions occur in applications that include faulted vapor compression systems, cold climate heat pumps, air conditioner start-up and shutdown processes, pump down operation of refrigeration systems, etc.

In the future, the uncertainty calculation framework in this paper will be used to compare the extrapolation capability of different types of compressor models to examine if models using more physical rules are more reliable in extrapolation cases. The framework will also be used to develop a general rule of thumb to determine when an extrapolation case is acceptable for different types of compressor models and compressors.

Nomenclature

β	Coefficient of a 10-coefficient map [unit varies]
COV	Coefficient of variation [dimensionless]
ε	Error between true value and estimation of a variable from a linear model [unit varies]
Δ	Uncertainty of a variable [unit varies]
m	Number of coefficients of 10-coefficient map [dimensionless]
n	Number of training data points [dimensionless]
P	Pressure [kPa]
r	Relative uncertainty [dimensionless]
σ	Mean square error [W]
T	Temperature [K]
$t_{n-m,0.95}$	Student's t value for a 95% confidence interval of estimates from equations with n training data

	points and m coefficients
$\dot{W}$	Power consumption [W]
x	Independent variable [unit varies]
X	Matrix of independent variables [unit varies]
y	Dependent variable [unit varies]

Accent

$\rightarrow$	Vectorized
$\hat{}$	Estimated

Subscript

close	Closest operating point on the boundary of the training data of a compressor map
comp	Compressor
corr	Correlated
dew	Dew point
dis	Discharge
EOS	Equation of state
exp	Expanded
full	Full-scale
high	High-order
i	i^{th} entry of a variable or coefficient
input	Uncertainty due to input
j	j^{th} entry of a variable
low	Low-order
max	Maximum
mea	Measured
min	Minimum
model	Uncertainty due to model random error
output	Uncertainty due to output
P	Pressure transducer
std	Standard
suc	Suction
train	Training data
true	True model of linear regression
uncorr	Uncorrelated

References

AHRI. (2004). ANSI/AHRI Standard 540: 2004 Standard for Performance Rating of Positive Displacement Refrigerant Compressors and Compressor Units. Arlington: Air-Conditioning, Heating, and Refrigeration Institute.

AHRI. (2016). Final Low-GWP AREP Test Reports. Retrieved September 21, 2016, from http://www.ahrinet.org/Resources/Research/AHRI-Low-GWP-Alternative-Refrigerants-Evaluation-Program/Reports-by-Category.aspx#Comp

ASHRAE. (2010a). ANSI/ASHRAE Guideline 2-2010: Engineering Analysis of Experimental Data. Atlanta: American Society of Heating, Refrigerating and Air-Conditioning Engineers, Inc.

ASHRAE. (2010b). ANSI/ASHRAE Standard 23.1-2010: Methods of Testing for Rating the Performance of Positive Displacement Refrigerant Compressors and Condensing Units That Operate at Subcritical Temperatures. Atlanta: American Society of Heating, Refrigerating and Air-Conditioning Engineers, Inc.

ASHRAE. (2014). ASHRAE Guideline 14-2014: Measurement of Energy, Demand, and Water Savings. Atlanta: American Society of Heating, Refrigerating and Air-Conditioning Engineers, Inc.

ASME. (2006). ASME V&V 10-2006 Guide for Verification and Validation in Computational Solid Mechanics. New York: American Society of Mechanical Engineers.

ASME. (2013). ASME PTC 19.1-2013: Test Uncertainty Performance Test Codes. New York: American Society of Mechanical Engineers.

Aute, V., Martin, C., & Radermacher, R. (2015). A Study of Methods to Represent Compressor Performance Data over an Operating Envelope Based on a Finite Set of Test Data (No. 8013). College Park, MD: Air-Conditioning, Heating, and Refrigeration Institute.

Bach, C. K., & Cheung, H. (2016). Mapping of Vapor Injected Compressor with Consideration of Extrapolation Uncertainty. ASHRAE Orlando 2016 Conference Paper. Orlando: American Society of Heating, Refrigerating and Air-Conditioning Engineers, Inc.

Bach, C. K., Groll, E. A., & Braun, J. E. (2016). Dual port vapor injected compression: In-system testing versus test stand testing, and mapping of results. *Renewable Energy*, 819-833.

Bell, I. H., Lemort, V., Groll, E. A., Braun, J. E., King, G. B., & Horton, W. T. (2012). Liquid-flooded compression and expansion in scroll machines – Part I: Model development. *International Journal of Refrigeration*, 35(7), 1878–1889.

Bell, I. H., Wronski, J., Quoilin, S., & Lemort, V. (2014). Pure and Pseudo-pure Fluid Thermophysical Property Evaluation and the Open-Source Thermophysical Property Library CoolProp. Industrial and Engineering Chemistry Research, 53(6), 2498-2508.

Caskey, S., Kultgen, D., Groll, E., Hutzel, W., & Menzi, T. (2012). Simulation of an Air-Source Heat Pump with Two-Stage Compression and Economizing for Cold Climates. *International Refrigeration and Air Conditioning Conference*.

CEN. (2013). EN 12900: Refrigerant Compressors - Rating Conditions, Tolerances and Presentation of Manufacturer's Performance Data. Brussels: European Committee for Standardisation.

Cheung, H., & Bach, C. K. (2015). Prediction of Uncertainty of 10-coefficient Compressor Maps for Extreme Operating Conditions. *IOP Conference Series: Materials Science and Engineering*. 90(1), p. 012078. IOP Publishing.

Cheung, H., & Braun, J. E. (2013). Simulation of fault impacts for vapor compression systems by inverse modeling. Part II: System modeling and validation. *HVAC&R Research*, 19(7), 907–921.

Coleman, H. W., & Steele, W. G. (2009). Experimentation, Validation, and Uncertainty Analysis for Engineers (3 edition). Hoboken, N.J: Wiley.

Dardenne, L., Fraccari, E., Maggioni, A., Molinaroli, L., Proserpio, L., & Winandy., E. (2015). Semi-Empirical Modelling of a Variable Speed Scroll Compressor with Vapour Injection. *International Journal of Refrigeration*, 54, 76-87.

Ding, G. (2007). Recent developments in simulation techniques for vapour-compression refrigeration systems. *International Journal of Refrigeration*, 30(7), 1119–1133.

Gall, J., Fisher, D. E., Corti, G., Marelli, S., & Cremaschi, L. (2015). Modeling of R-410A variable capacity compressor with Modelica and experimental validation. *International Journal of Refrigeration*, 58, 90-109.

Heo, J., Yun, R., & Kim, Y. (2013). Simulations on the performance of a vapor-injection heat pump for different cylinder volume ratios of a twin rotary compressor. *International Journal of Refrigeration*, 36(3), 730–744.

Ibsaine, R., Joffroy, J.-M., & Stouffs, P. (2016). Modelling of a new thermal compressor for supercritical CO2 heat pump. Energy.

Jähnig, D. I., Reindl, D. T., & Klein, S. A. (2000). A Semi-Empirical Method for Representing Domestic Refrigerator/Freezer Compressor Calorimeter Test Data. *ASHRAE Transactions*, 106(2), 122–130.

JCGM. (2008). JCGM 100:2008: Evaluation of Measurement Data – Guide to the Expression of Uncertainty in Measurement. *Joint Committee for Guides in Metrology*.

Kamei, A., Beyerlein, S. W., & Jacobsen, R. T. (1995). Application of Nonlinear Regression in the Development of a Wide Range Formation for HCFC-22. *International Journal of Thermophysics*, 16(5), 1155 – 1164.

Kennedy, M. C., & O'Hagan, A. (2001). Bayesian Calibration of Computer Models. *Journal of the Royal Statistical Society: Series B (Statistical Methodology)*, 63(3), 425 - 464.

Lemmon, E. W. (2003). Pseudo-Pure Fluid Equations of State for the Refrigerant Blends R-410A, R-404A, R-507C, and R-407C. *International Journal of Thermophysics*, 24(4), 991 - 1006.

Li, W. (2012). Simplified steady-state modeling for hermetic compressors with focus on extrapolation. *International Journal of Refrigeration*, 35(6), 1722–1733.

Moffat, R. J. (1988). Describing the uncertainties in experimental results. *Experimental Thermal and Fluid Science*, 1(1), 3–17.

Molinaroli, L., Joppolo, C. M., & De Antonellis, S. (2017). A Semi-Empirical Model for Hermetic Rolling Piston Compressors. *International Journal of Refrigeration*, doi:10.1016/j.ijrefrig.2017.04.015.

Montgomery, D. (2005). Design and Analysis of Experiments, 6th Edition. Jon Wiley & Sons.

Navarro, E., Redón, A., Gonzálvez-Macia, J., Martinez-Galvan, I., & Corberán, J. (2013). Characterization of a Vapor Injection Scroll Compressor as a Function of Low, Intermediate and High Pressures and Temperature Conditions. *International Journal of Refrigeration*, 36(7), 1821–1829.

Park, Y. C., Kim, Y. C., & Min, M.-K. (2001). Performance analysis on a multi-type inverter air conditioner. *Energy Conversion and Management*, 42(13), 1607–1621.

Rasmussen, B. P. (2012). Dynamic modeling for vapor compression systems—Part I: Literature review. *HVAC&R Research*, 18(5), 934–955.

Rice, C. K., & Jackson, W. L. (2005). DOE/ORNL Heat Pump Design Model on the Web, Mark VII Version. Retrieved September 21, 2016, from http://web.ornl.gov/~wlj/hpdm/MarkVII.shtml

Roy, C. J., & Oberkampf, L. W. (2011). A comprehensive framework for verification, validation, and uncertainty quantification in scientific computing. *Computer Methods in Applied Mechanics and Engineering*, 200, 2131 – 2144.

Ruch, D. K., & Claridge, D. E. (1993). A Development and Comparison of NAC estimates for Linear and Change-point Energy Models for Commercial Buildings. *Energy and Buildings*, 20, 87 – 95.

Shao, S., Shi, W., Li, X., & H., C. (2004). Performance representation of variable-speed compressor for inverter air conditioners based on experimental data. *International Journal of Refrigeration*, 27, 805 - 815.

Shen, B., Braun, J. E., & Groll, E. A. (2009). Improved methodologies for simulating unitary air conditioners at off-design conditions. *International Journal of Refrigeration*, 32(7), 1837–1849.

Shrestha, S., Mahderekal, I., Sharma, V., & Abdelaziz, O. (2013a). Compressor Calorimeter Test of R-410A Alternatives R-32, DR-5, And L-41a. *Oak Ridge: Oak Ridge National Laboratory*.

Shrestha, S., Sharma, V., & Abdelaziz, O. (2013b). Compressor Calorimeter Test of R-404A Alternatives ARM-31a, D2Y-65, L-40, and R32+ R-134a Mixture using a Scroll Compressor. *Oak Ridge: Oak Ridge National Laboratory*.

Thorade, M., & Saadat., A. (2013). Partial derivatives of thermodynamic state properties for dynamic simulation. *Environmental Earth Sciences*, 70(8), 3497-3503.

Wang, S., Wang, J., & Burnett, J. (2000). Mechanistic model of centrifugal chillers for HVAC system dynamics simulation. *Building Services Engineering Research and Technology*, 21(2), 73–83.

Wang, B., Shi, W., Li, X., & Yan., Q. (2008). Numerical Research on the Scroll Compressor with Refrigeration Injection. *Applied Thermal Engineering*, 28, 440-449.

Winandy, E., O., C. S., & Lebrun, J. (2002). Experimental Analysis and Simplified Modelling of a Hermetic Scroll Refrigeration Compressor. *Applied Thermal Engineering*, 220, 107-120.

Zakula, T., Gayeski, N. T., Armstrong, P. R., & Norford, L. K. (2011). Variable-speed heat pump model for a wide range of cooling conditions and loads. *HVAC&R Research*, 17(5), 670–691.

Appendix A Analytical Calculation of Partial Derivatives with Respect to Training Data Points in Eq. (17) and (18)

This appendix describes the analytical derivation of the formula to calculate the partial derivatives of coefficients with respect to training data observations in Eq. (17) and (18).

Calculating partial derivatives of coefficients with respect to training data observations of compressor power consumption

To calculate the partial derivative, the product rule can be used to split the derivative of coefficients as Eq. (29).

$$\frac{\partial \vec{\beta}}{\partial \dot{W}_{comp,train,j}} = \frac{\partial \vec{\beta}}{\partial \vec{W}_{train}} \frac{\partial \vec{W}_{train}}{\partial \dot{W}_{comp,train,j}} \tag{29}$$

where j means the jth entry in the vector $\vec{W}_{train}$

The first partial derivative in Eq. (29) can be calculated from the estimation equation of the coefficients as Eq. (30).

$$\frac{\partial \vec{\beta}}{\partial \vec{W}_{train}} = (X_{train}^T X_{train})^{-1} X_{train}^T \tag{30}$$

The second derivative in Eq. (29) is a zero vector except the jth entry which is one, and $\frac{\partial \beta_i}{\partial W_{comp,train,j}}$ in Eq. (17) and (18) is the ith entry in the vector $\frac{\partial \vec{\beta}}{\partial W_{comp,train,j}}$.

Calculating partial derivative of coefficients with respect to training data observations of compressor suction and discharge dew point temperature

By matrix calculus, the partial derivative of coefficients with respect to a compressor suction dew point temperature in the training data can be obtained by differentiating Eq. (3) into multiple parts as Eq. (31) to (34).

$$\frac{\partial \vec{\beta}}{\partial T_{dew,suc,j}} = \left[\frac{\partial (X_{train}^T X_{train})^{-1}}{\partial T_{dew,suc,j}} X_{train}^T + (X_{train}^T X_{train})^{-1} \frac{\partial X_{train}^T}{\partial T_{dew,suc,j}} \right] \vec{W}_{comp,train} \tag{31}$$

$$\frac{\partial (X_{train}^T X_{train})^{-1}}{\partial T_{dew,suc,j}} = -(X_{train}^T X_{train})^{-1} \frac{\partial (X_{train}^T X_{train})}{\partial T_{dew,suc,j}} (X_{train}^T X_{train})^{-1} \tag{32}$$

$$\frac{\partial(X_{train}^T X_{train})}{\partial T_{dew,suc,j}} = \frac{\partial X_{train}^T}{\partial T_{dew,suc,j}} X_{train} + X_{train}^T \frac{\partial X_{train}}{\partial T_{dew,suc,j}} \tag{33}$$

$$\frac{\partial X_{train}^T}{\partial T_{dew,suc,j}} = \left(\frac{\partial X_{train}}{\partial T_{dew,suc,j}}\right)^T \tag{34}$$

$\frac{\partial X_{train}}{\partial T_{dew,suc,j}}$ is a matrix with zero values except its jth row as shown in Eq. (35).

$$\frac{\partial X_{train}}{\partial T_{dew,suc,j}} = \begin{bmatrix} & & & & 0 & \cdots & 0 & & & \\ & & & & & \vdots & & & & \\ 0 & 1 & 0 & 2T_{dew,suc,j} & T_{dew,dis,j} & 0 & 3T_{dew,suc,j}^2 & 2T_{dew,suc,j}T_{dew,dis,j} & T_{dew,dis,j}^2 & 0 \\ & & & & & \vdots & & & & \\ & & & & 0 & \cdots & 0 & & & \end{bmatrix} \tag{35}$$

The partial derivative of the ith coefficient with respect to the jth compressor suction dew point temperature in the training data can be obtained by selecting the ith entry in the partial derivative of the coefficient vector in Eq. (31).

The partial derivative of the coefficient vector with respect to compressor discharge dew point temperature in training data can be obtained by substituting the compressor suction dew point temperature from Eq. (31) to (34) by compressor discharge dew point temperature and calculating $\frac{\partial X_{train}}{\partial T_{dew,dis,j}}$ by Eq. (36).

$$\frac{\partial X_{train}}{\partial T_{dew,dis,j}} = \begin{bmatrix} & & & & 0 & \cdots & 0 & & & \\ & & & & & \vdots & & & & \\ 0 & 0 & 1 & 0 & 2T_{dew,dis,j} & T_{dew,dis,j} & 0 & T_{dew,suc,j}^2 & 2T_{dew,suc,j}T_{dew,dis,j} & 3T_{dew,dis,j}^2 \\ & & & & & \vdots & & & & \\ & & & & 0 & \cdots & 0 & & & \end{bmatrix} \tag{36}$$

Appendix B Parity Plots of Measured and Estimated Power Consumption of Different Compressor Maps Calibrated by Different Sets of Training Data

This appendix includes the parity plots of the compressor maps to compare the measured and estimated compressor power consumption that are not included in the main body of the paper for readers' reference.
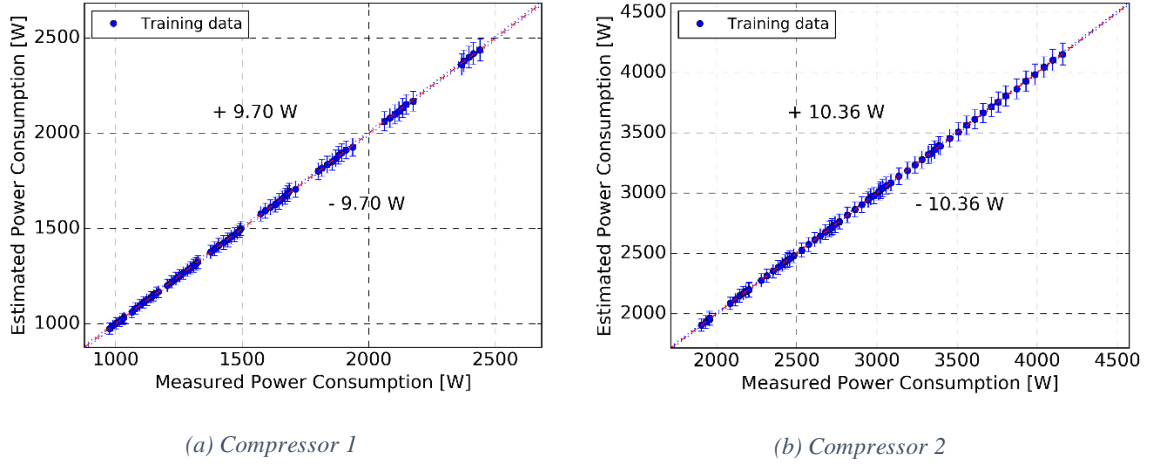
(a) Compressor 1   *(b) Compressor 2*

Figure 11: Comparison between measured and estimated power consumption for the Map from All Data Set of both compressors with overall expanded uncertainty of map outputs
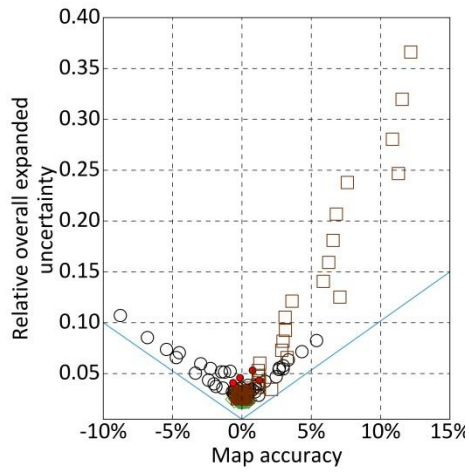

(a) Compressor 1   *(b) Compressor 2*
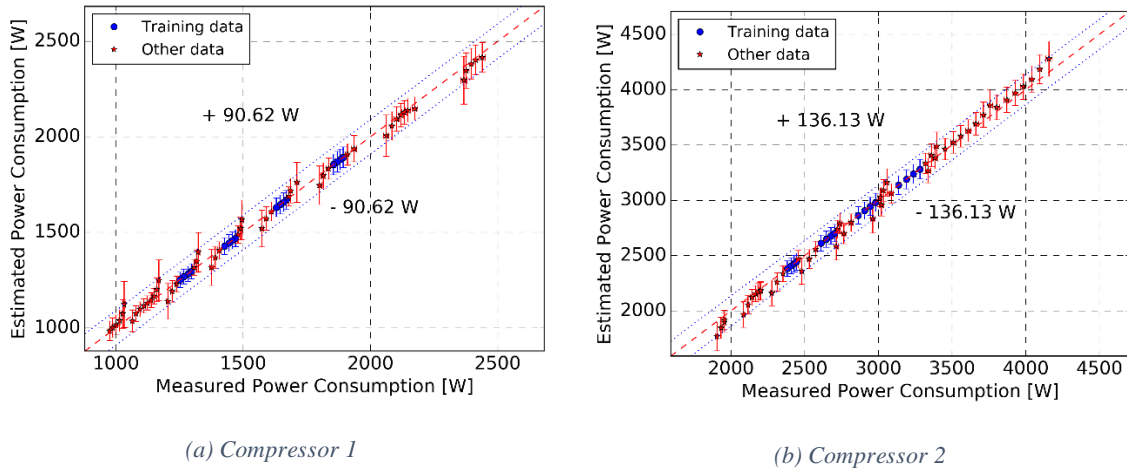
Figure 12: Comparison between measured and estimated power consumption for the Map from Set Mid of both compressors with overall expanded uncertainty of map outputs
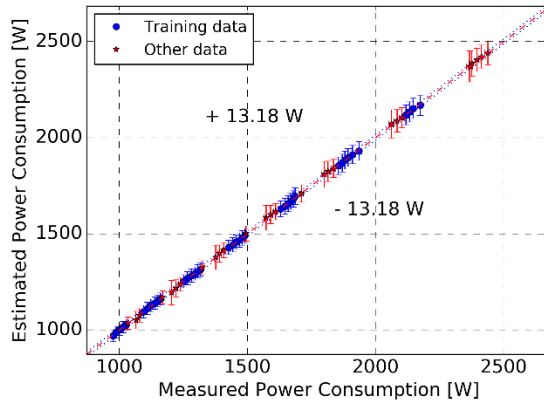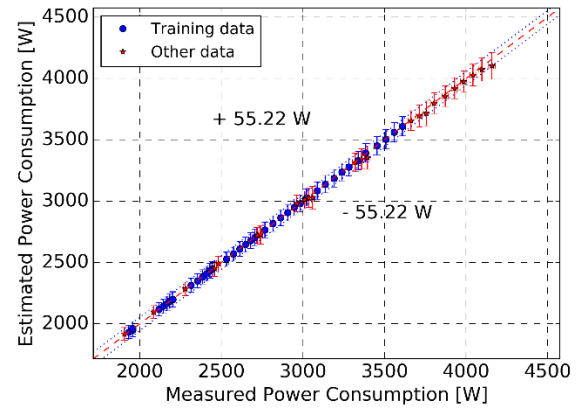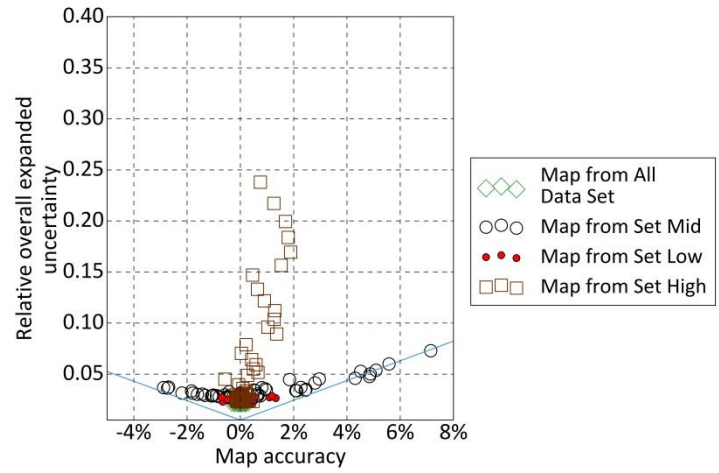
(a) Compressor 1

(b) Compressor 2

Figure 13: Comparison between measured and estimated power consumption for the Map from Set Low of both compressors with overall expanded uncertainty of map outputs

Figures

Figure 1: Flowchart of uncertainty propagation to the compressor map output
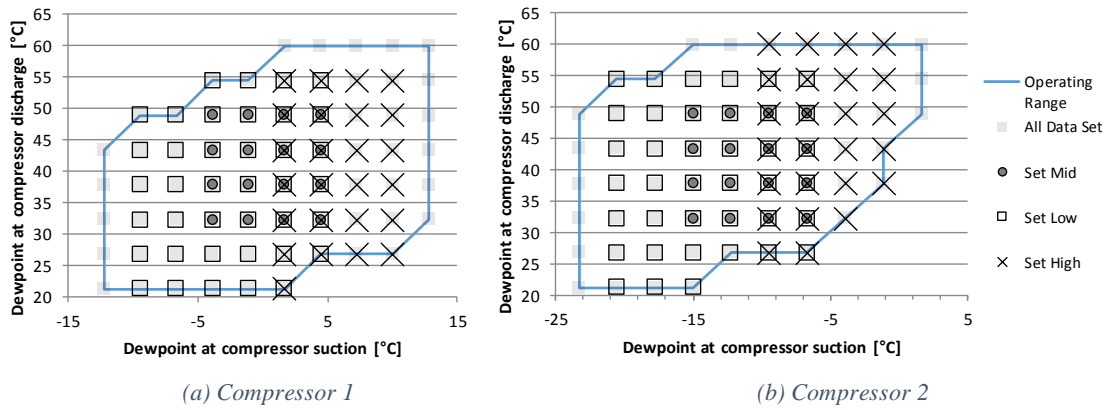
(a) Compressor 1   *(b) Compressor 2*

Figure 2: Operating conditions in compressors tests and the subsets defined for extrapolation uncertainty studies
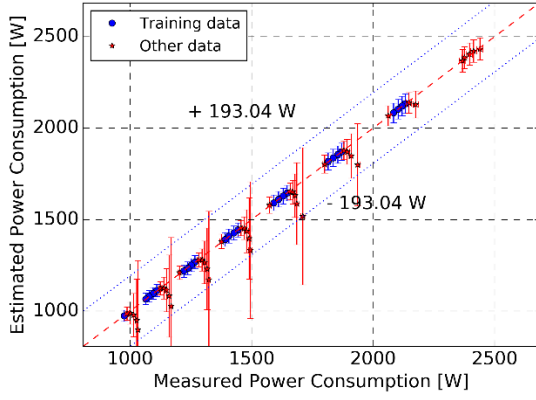
(a) Compressor 1   *(b) Compressor 2*
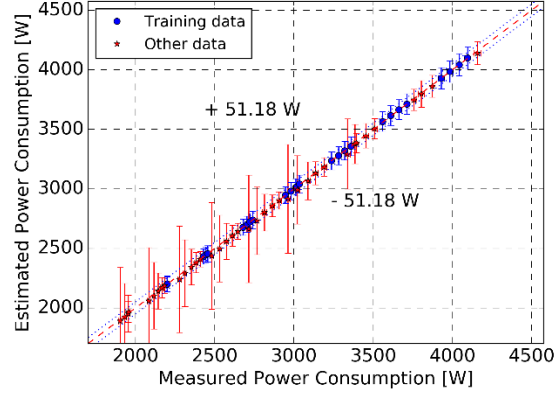
Figure 3: Comparison between measured and estimated power consumption for the map from Set High of both compressors with overall expanded uncertainty of map outputs
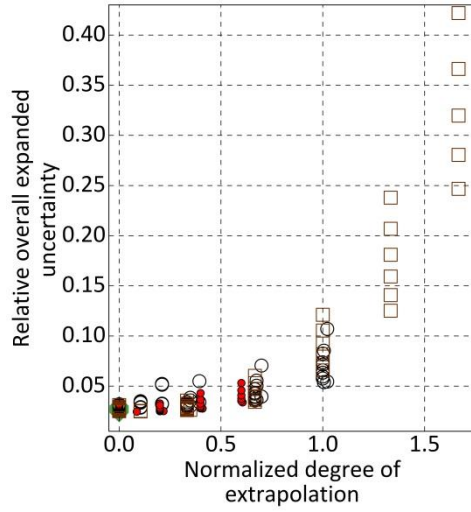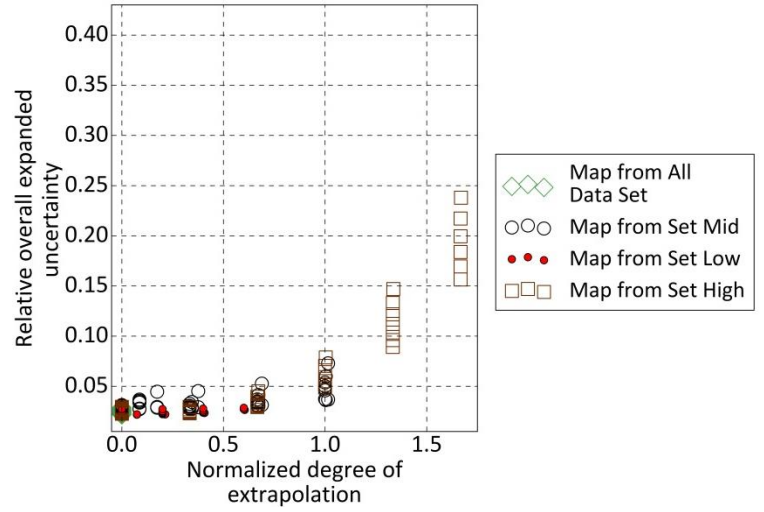
(a) Compressor 1   *(b) Compressor 2*

Figure 4: Change of relative overall expanded uncertainty with normalized degree of extrapolation for all maps

(a) Compressor 1   *(b) Compressor 2*

Figure 5: Change of relative overall expanded uncertainty with map accuracy in all maps

(a) Compressor 1

(b) Compressor 2

Figure 6: Change of uncertainty components in map outputs with normalized degree of extrapolation in all maps
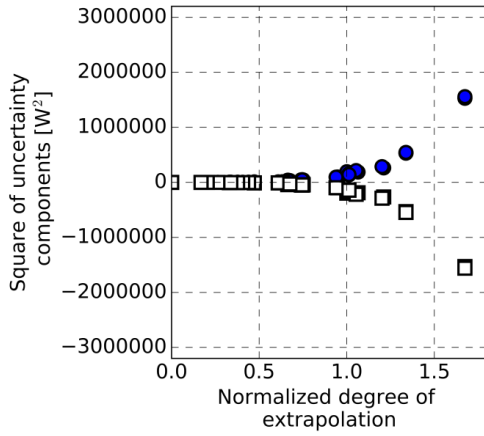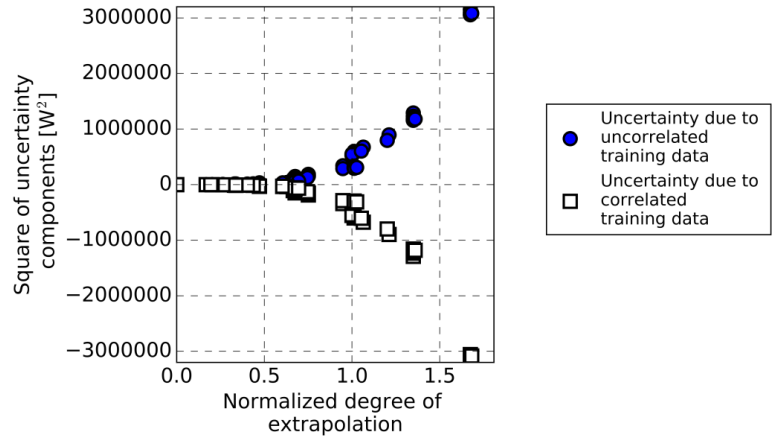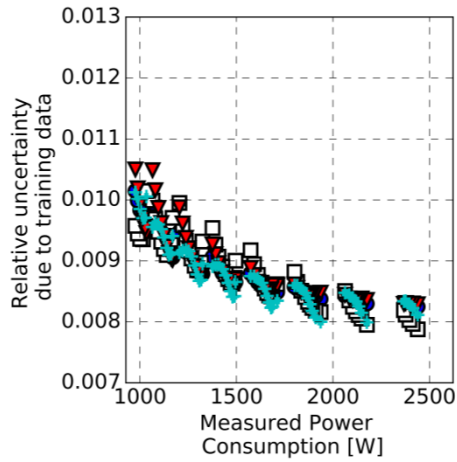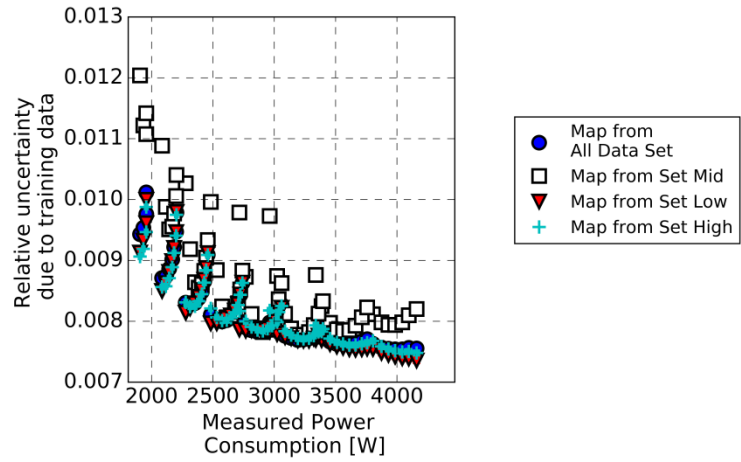
(a) Compressor 1

(b) Compressor 2

Figure 7: Change of components of uncertainty due to training data in map outputs with normalized degree of extrapolation in all maps
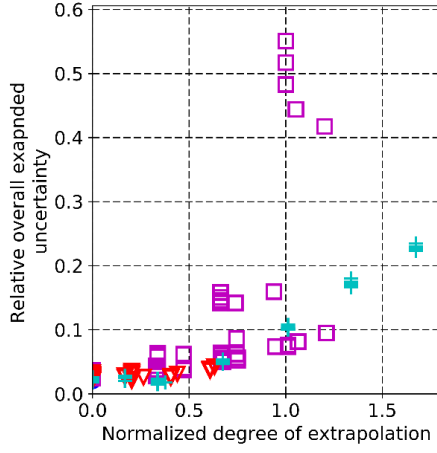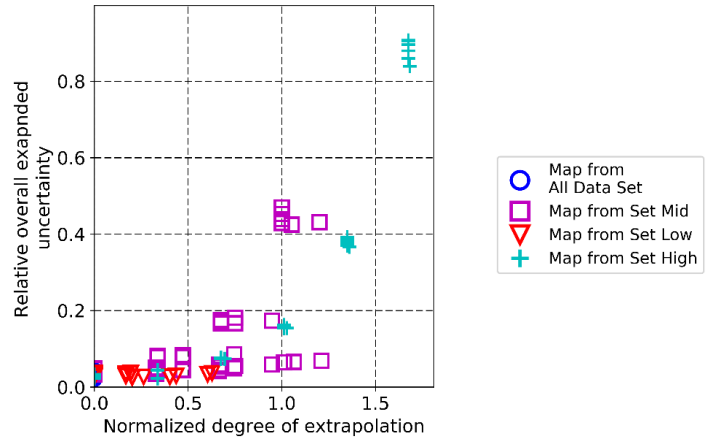

(a) Compressor 1

(b) Compressor 2

Figure 8: Comparison of uncertainties due to training data from different maps at all operating conditions
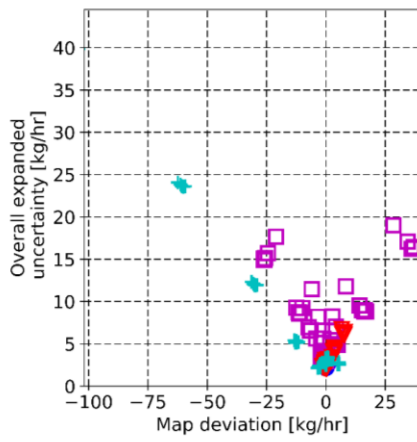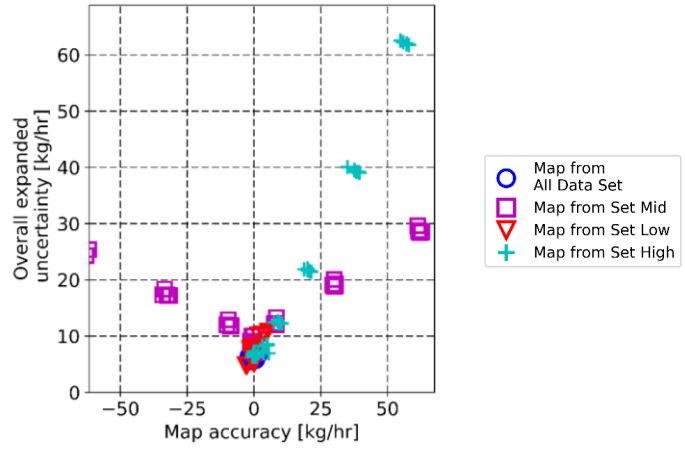
(a) Compressor 1

(b) Compressor 2

Figure 9: Change of relative overall expanded uncertainty with normalized degree of extrapolation for all maps estimating refrigerant mass flow rates
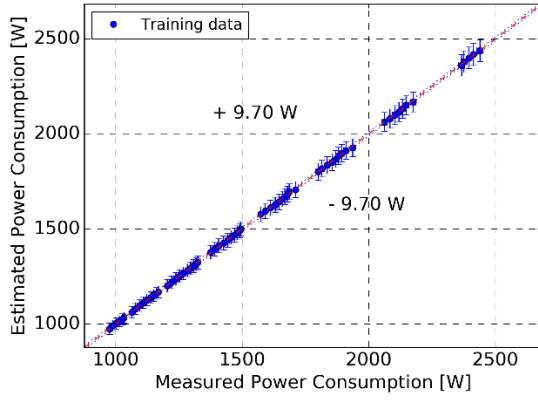

(a) Compressor 1

(b) Compressor 2

Figure 10: Change of overall expanded uncertainty with map deviation in all maps estimating refrigerant mass flow rate

(a) Compressor 1 *(b) Compressor 2*
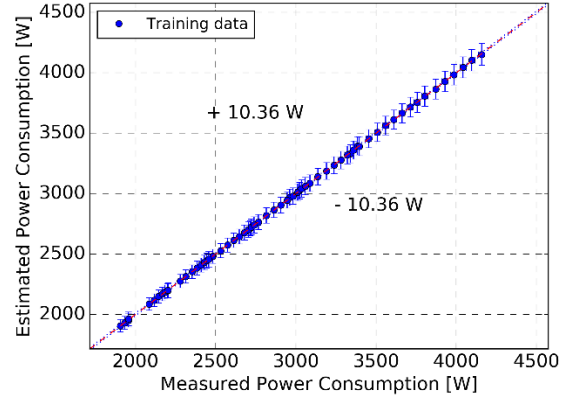
Figure 11: Comparison between measured and estimated power consumption for the Map from All Data Set of both compressors with overall expanded uncertainty of map outputs

(a) Compressor 1 *(b) Compressor 2*

Figure 12: Comparison between measured and estimated power consumption for the Map from Set Mid of both compressors with overall expanded uncertainty of map outputs

(a) Compressor 1
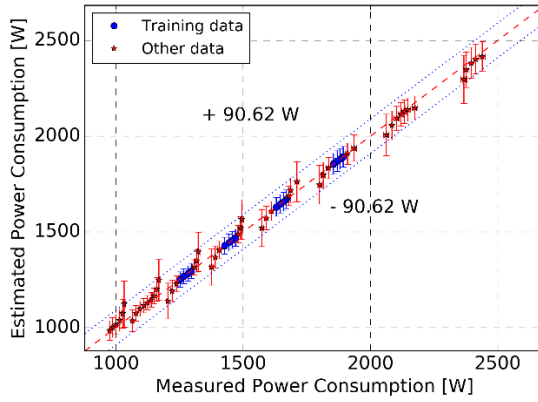
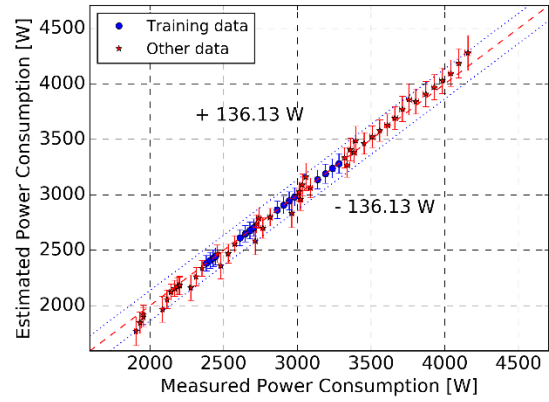*(b) Compressor 2*

Figure 13: Comparison between measured and estimated power consumption for the Map from Set Low of both compressors with overall expanded uncertainty of map outputs
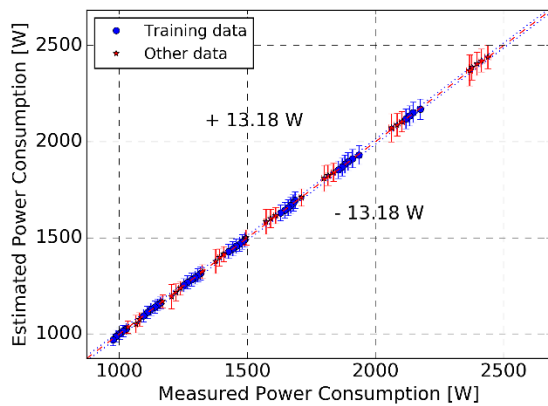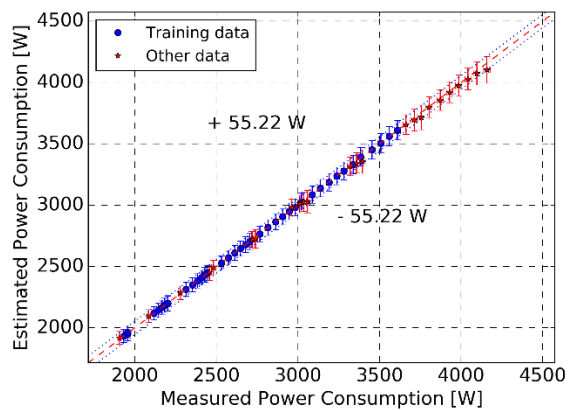
Tables

<table>
<tr><td colspan="3">Table 1: Uncertainty of equations of states of different refrigerant</td></tr>
<tr><td>Refrigerant</td><td>Uncertainty</td><td>Literature</td></tr>
<tr><td>R22</td><td>0.2% of the dew point pressure</td><td>Kamei et al. (1995)</td></tr>
<tr><td>R404A</td><td>0.5% of the dew point pressure</td><td>Lemmon (2003)</td></tr>
<tr><td>R410A</td><td>0.5% of the dew point pressure</td><td>Lemmon (2003)</td></tr>
</table>

<table>
<tr><td colspan="3">Table 2: Specification of compressors</td></tr>
<tr><td>Specification</td><td>Compressor 1
(Shrestha et al. 2013a)</td><td>Compressor 2
(Shrestha et al. 2013b)</td></tr>
<tr><td>Compressor type</td><td colspan="2">Hermetic scroll</td></tr>
<tr><td>Frequency [Hz]</td><td colspan="2">60</td></tr>
<tr><td>Voltage [V]</td><td colspan="2">208/230</td></tr>
<tr><td>Displacement volume [cm^3 rev^{-1}]</td><td>20.3</td><td>51.0</td></tr>
<tr><td>Refrigerant</td><td>R410A</td><td>R404A</td></tr>
<tr><td>Rated power consumption [W]</td><td>2170</td><td>3320</td></tr>
<tr><td>Superheat [K]</td><td colspan="2">11.1</td></tr>
</table>

<table>
<tr><td colspan="4">Table 3: Uncertainties of sensors used in the setup</td></tr>
<tr><td>Sensors</td><td>Locations</td><td>Measurement range</td><td>Uncertainty</td></tr>
<tr><td>Power energy meter</td><td>Compressor power consumption</td><td>Not available from the data source</td><td>±0.5% of the measured value</td></tr>
<tr><td>Pressure transmitter 1</td><td>Compressor discharge</td><td>0 – 5170 kPa</td><td>±0.25% full scale</td></tr>
<tr><td>Pressure transmitter 2</td><td>Compressor suction</td><td>0 – 1380 kPa</td><td>±0.25% full scale</td></tr>
<tr><td>Refrigerant mass flowmeter</td><td>Condenser outlet</td><td>Not available from the data source</td><td>±0.10% of the measured value</td></tr>
</table>

<table>
<tr><td colspan="6">Table 5: Coefficients of variation over their training data points for all trained compressor maps</td></tr>
<tr><td>Compressor 1</td><td>Coefficient of variation</td><td>Number of training data points</td><td>Compressor 2</td><td>Coefficient of variation</td><td>Number of training data points</td></tr>
<tr><td>Map from All Data Set</td><td>0.0021</td><td>66</td><td>Map from All Data Set</td><td>0.0013</td><td>63</td></tr>
<tr><td>Map from Set Mid</td><td>0.0004</td><td>16</td><td>Map from Set Mid</td><td>0.0002</td><td>16</td></tr>
<tr><td>Map from Set Low</td><td>0.0021</td><td>39</td><td>Map from Set Low</td><td>0.0012</td><td>39</td></tr>
<tr><td>Map from Set High</td><td>0.0010</td><td>25</td><td>Map from Set High</td><td>0.0007</td><td>25</td></tr>
</table>